LEVEL

(12)

ANALYSIS OF THE SUPERPOSITION OF GROUND MOTIONS FROM A SURFACE ROW-CRATERING EXPERIMENT AND SINGLE CONTAINED NUCLEAR EVENTS

AD A070051

DDC RECEIVED JUN 18 1979 C

FINAL TECHNICAL REPORT

This research was supported by the
Advanced Research Projects Agency of the Department of Defense
and was monitored by AFTAC/VSC, Patrick AFB, Florida. 32925.

JANUARY 1979

DDC FILE_COPY

Prepared by:

R. D. LYNCH

COMPUTER SCIENCES CORPORATION
6565 Arlington Boulevard
Falls Church, Virginia 22046

CONTRACT NO.:	F08606-78-C-0008
EFFECTIVE DATE OF CONTRACT:	OCTOBER 1, 1977
CONTRACT EXPIRATION DATE:	JANUARY 31, 1979
ARPA ORDER NO.:	02551
PROGRAM CODE:	8F1000
AFTAC PROJECT AUTHORIZATION NO.:	VT/8704
AFTAC PROJECT SCIENTIST:	MICHAEL J. SHORE

ANALYSIS OF THE SUPERPOSITION OF GROUND MOTIONS FROM A SURFACE ROW-CRATERING EXPERIMENT AND SINGLE CONTAINED NUCLEAR EVENTS

FINAL TECHNICAL REPORT

This research was supported by the
Advanced Research Projects Agency of the Department of Defense
and was monitored by AFTAC/VSC, Patrick AFB, Florida. 32925.

JANUARY 1979

Prepared by:

R. D. LYNCH

COMPUTER SCIENCES CORPORATION
6565 Arlington Boulevard
Falls Church, Virginia 22046

CONTRACT NO.:	F08606-78-C-0008
EFFECTIVE DATE OF CONTRACT:	OCTOBER 1, 1977
CONTRACT EXPIRATION DATE:	JANUARY 31, 1979
ARPA ORDER NO.:	02551
PROGRAM CODE:	8F1000
AFTAC PROJECT AUTHORIZATION NO.:	VT/8704
AFTAC PROJECT SCIENTIST:	MICHAEL J. SHORE

UNCLASSIFIED

SECURITY CLASSIFICATION OF THIS PAGE (When Data Entered)

REPORT DOCUMENTATION PAGE		READ INSTRUCTIONS BEFORE COMPLETING FORM
1. REPORT NUMBER	2. GOVT ACCESSION NO.	3. RECIPIENT'S CATALOG NUMBER
4. TITLE (and Subtitle) Analysis of the Superposition of Ground Motions from a Surface Row-Cratering Experiment and Single Contained Nuclear Events.		5. TYPE OF REPORT & PERIOD COVERED Final Technical Report. 1 Oct 77 - 31 Jan 79,
		6. PERFORMING ORG. REPORT NUMBER
7. AUTHOR(s) R. D. Lynch		8. CONTRACT OR GRANT NUMBER(s) F08606-78-C-0008, ARPA Order 02551
9. PERFORMING ORGANIZATION NAME AND ADDRESS Computer Sciences Corporation 6565 Arlington Boulevard Falls Church, Virginia 22046		10. PROGRAM ELEMENT, PROJECT, TASK AREA & WORK UNIT NUMBERS ARPA Order No. 02551 Program Code 8F1000
11. CONTROLLING OFFICE NAME AND ADDRESS		12. REPORT DATE 31 January 1979
		13. NUMBER OF PAGES 70p.
14. MONITORING AGENCY NAME & ADDRESS (if different from Controlling Office) AFTAC/VSC Patrick AFB, Florida 32925		15. SECURITY CLASS. (of this report) UNCLASSIFIED
		15a. DECLASSIFICATION/DOWNGRADING SCHEDULE

16. DISTRIBUTION STATEMENT (of this Report)

Approved for Public Release, Distribution Unlimited

17. DISTRIBUTION STATEMENT (of the abstract entered in Block 20, if different from Report)

18. SUPPLEMENTARY NOTES

19. KEY WORDS (Continue on reverse side if necessary and identify by block number)

Seismic
Ground Motion
PNE Evasion Scenario

20. ABSTRACT (Continue on reverse side if necessary and identify by block number)

This report examines the seismic aspects of a Threshold Test Ban Treaty Evasion scenario in which a clandestine nuclear device is detonated in the environment of a Peaceful Nuclear Experiment (PNE) involving the simultaneous detonation of a near-surface, multiple nuclear device configuration. The yield, location, and detonation delay time of the clandestine event relative to the PNE are examined in terms of the constraints imposed by both on-site and far-field monitoring equipment. Seismic recordings from the near-surface multiple detonation event, Buggy I, are used for the PNE while seismic recordings for the

DD FORM 1 JAN 73 1473 EDITION OF 1 NOV 65 IS OBSOLETE

405717

UNCLASSIFIED

SECURITY CLASSIFICATION OF THIS PAGE (When Data Entered)

20. Abstract (continued)
clandestine event are obtained by yield scaling the ground motion recordings from single contained events having the appropriate source-to-receiver distance. These two classes of signals are superimposed to simulate the ground motion for an evasion scenario. Spectral information is obtained from the PNE and the superposition seismograms and then analyzed to quantify the effect caused by the clandestine event.

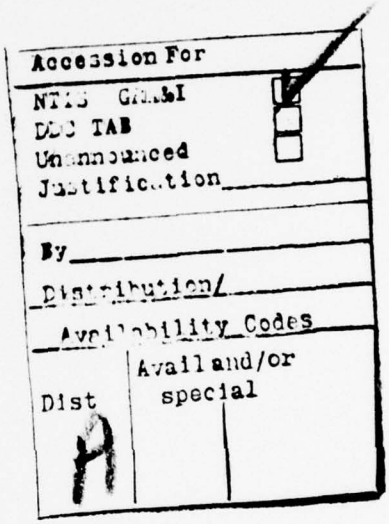

TABLE OF CONTENTS

		Page
1.	INTRODUCTION	1-1
2.	EXAMINATION OF THE CONSTRAINTS ON THE YIELD, LOCATION, AND DETONATION TIME OF THE CLANDESTINE EVENT	2-1
	2.1 Introduction	2-1
	2.2 Constraints on Yield	2-1
	2.3 Constraints on the Clandestine Event Location and Detonation Delay Time	2-2
3.	COMPARISON ON A SURFACE ROW-CRATERING EVENT WITH SINGLE CONTAINED EVENTS OF EQUIVALENT YIELD	3-1
	3.1 Introduction	3-1
	3.2 The Surface Row-Cratering Event	3-1
	3.3 Single Contained Events	3-3
	3.4 Comparison of the Seismic Characteristics of a Surface Row-Cratering Event and Single Contained Events of Equivalent Yield	3-4
4.	SIMULATION AND ANALYSIS OF THE PNE EVASION SCENARIO	4-1
	4.1 Introduction	4-1
	4.2 Data Sample	4-1
	4.3 Superposition of Scaled Almendro and Buggy I	4-4
	4.4 Superpositions Involving Seismograms from Four Events	4-22
5.	SUMMARY, CONCLUSIONS AND RECOMMENDATIONS	5-1
	5.1 Summary and Conclusions	5-1
	5.2 Recommendations	5-2
	REFERENCES	R-1

LIST OF FIGURES

Figure		Page
2.1	Teleseismic Discrimination of Two Seismic Sources Based on Source Separation, Detonation Delay Time and Teleseismic Distance	2-7
3.1	The Location of the Seismic Recording Stations Relative to the Buggy I Event	3-2
3.2	A Plot of the Peak Velocity Versus Distance for Buggy I (Circles) and Single Contained Events (Dots)	3-6
3.3	An Example of An Amplitude Spectra Obtained Using the Narrow-Band Filter Technique	3-7
3.4	Spectral Amplitude Versus Distance for Buggy I Circles and Single Contained Events (DOTS)	3-10
3.5	A Plot for the Average Spectral Ratio of Single Contained Events to Buggy I	3-11
4.1	Seismograms from Buggy I, Station 447 (Top Trace); Scaled Almendro (1.375 kt), Station L03 (Middle Trace); and the Superposition (Bottom Trace)	4-5
4.2	Seismograms from Buggy I, Station 447 (Top Trace); Scaled Almendro (1.375 kt), Station L04 (Middle Trace); and the Superposition (Bottom Trace)	4-6
4.3	Seismograms from Buggy I, Station 458 (Top Trace); Scaled Almendro (1.375 kt), Station L03 (Middle Trace); and the Superposition (Bottom Trace)	4-7
4.4	Seismograms from Buggy I, Station 458 (Top Trace); Scaled Almendro (1.375 kt), Station L04 (Midde Trace); and Superposition (Bottom Trace)	4-8
4.5	Seismograms from Buggy I, Station 449 (Top Trace); Scaled Almendro (1.375 kt); Station L05 (Middle Trace); and the Superposition (Bottom Trace)	4-9
4.6	Seismograms from Buggy I, Station 449 (Top Trace); Scaled Almendro (1.375 kt); Station L02 (Middle Trace); and the Superposition (Bottom Trace)	4-10
4.7	Seismograms from Buggy I, Station 449 (Top Trace); Scaled Almendro (1.375 kt); Station A19T (Middle Trace); and the Superposition (Bottom Trace)	4-11

LIST OF FIGURES (Continued)

4.8 Seismograms from Buggy I, Station 450 (Top Trace); Scaled Almendro (1.375 k5) Station L06 (Middle Trace); and the Superposition (Bottom Trace) 4-12

4.9 Spectra from Buggy I, Station 447 (Dashed Curve) and the Superposition with Scaled Almendro, Station L03, 1.375 kt (Solid Curve) and 2.5 kt (Dotted Line) 4-13

4.10 Spectra from Buggy I, Station 447 (Dashed Curve) and the Superposition with Scaled Almendro, Station L04, 1.375 kt (Solid Curve) and 2.5 kt (Dotted Curve) 4-14

4.11 Spectra from Buggy I, Station 458 (Dashed Curve) and the Superposition with Scaled Almendro, Station L03, 1.375 kt (Solid Curve) and 2.5 kt (Dotted Curve) 4-15

4.12 Spectra from Buggy I, Station 458 (Dashed Curve) and the Superposition with Scaled Almendro, Station L04, 1.375 kt (Solid Curve) and 2.5 kt (Dotted Curve) 4-16

4.13 Spectra from Buggy I, Station 449 (Dashed Curve) and the Superposition with Scaled Almendro, Station L05, 1.375 kt (Solid Curve) and 2.5 kt (Dotted Curve) 4-17

4.14 Spectra from Buggy I, Station 449 (Dashed Curve) and the Superposition with Scaled Almendro, Station L02, 1.375 kt (Solid Curve) and 2.5 kt (Dotted Curve) 4-18

4.15 Spectra from Buggy I, Station 449 (Dashed Curve) and the Superposition with Scaled Almendro, Station A19T, 1.375 kt (Solid Curve) and 2.5 kt (Dotted Curve) 4-19

4.16 Spectra from Buggy I, Station 450 (Dashed Curve) and the Superposition with Scaled Almendro, Station L06, 1.375 kt (Solid Curve) and 2.5 kt (Dotted Curve) 4-20

4.17 A Plot of the Average Spectral Ratio of the Superpositions using Scaled Almendro to Buggy I, 1.375 kt (Dashed Curve) and 2.5 kt (Solid Curve) 4-21

4.18 Seismograms from Buggy I, Station 447 (Top Trace); Scaled Event A (2.5 kt), Station 790 (Middle Trace); and the Superposition (Bottom Trace) 4-23

LIST OF FIGURES (Continued)

4.19 Seismograms from Buggy I, Station 458 (Top Trace); Scaled Event A (2.5 kt), Station 750 (Middle Trace); and the Superposition (Bottom Trace) 4-24

4.20 Seismograms from Buggy I, Station 458 (Top Trace); Scaled Event A (2.5 kt), Station 780 (Middle Trace); and the Superposition (Bottom trace) 4-25

4.21 Seismograms from Buggy I, Station 458 (Top Trace); Scaled Event B (2.5 kt), Station L08 (Middle Trace); and the Superposition (Bottom Trace) 4-26

4.22 Seismograms from Buggy I, Station 449 (Top Trace); Scaled Event C (2.5 kt), Station 765 (Middle Trace); and the Superposition (Bottom trace) 4-27

4.23 Seismograms from Buggy I, Station 450 (Top Trace); Scaled Event D (2.5 kt), Station CP1 (Middle Trace); and the Superposition (Bottom Trace) 4-28

4.24 Spectra from Buggy I, Station 447 (Dashed Curve), and the Superposition with Scaled Event A, Station 790, 1.375 kt (Solid Curve) and 2.5 kt (Dotted Curve) 4-29

4.25 Spectra from Buggy I, Station 458 (Dashed Curve) and the Superposition with Scaled Event A, Station 750, 1.375 kt (Solid Curve) and 2.5 kt (Dotted Curve) 4-30

4.26 Spectra from Buggy I, Station 458 (Dashed Curve) and the Superposition with Scaled Event A, Station 780, 1.375 kt (Solid Curve) and 2.5 kt (Dotted Curve) 4-31

4.27 Spectra from Buggy I, Station 458 (Dashed Curve) and the Superposition with Scaled Event B, Station L08, 1.375 kt (Solid Curve) and 2.5 kt (Dotted Curve) 4-32

4.28 Spectra from Buggy I, Station 449 (Dashed Curve) and the Superposition with Scaled Event C, Station 765, 1.375 kt (Solid Curve) and 2.5 kt (Dotted Curve) 4-33

4.29 Spectra from Buggy I, Station 450 (Dashed Curve) and the Superposition with Scaled Event D, Station CP1, 1.375 kt (Solid Curve) and 2.5 kt (Dotted Curve) 4-34

4.30 A Plot of the Average Spectral Ratio of the Superpositions Using Four Scaled Events to Buggy I, 1.375 kt (Dashed Curve) and 2.5 kt (Solid Curve) . . 4-35

LIST OF TABLES

Table		Page
3.1	Estimated Parameter from the Analysis of Spectral Information from Single, Contained Events	3-9
4.1	General Event Information	4-2
4.2	Observed Peak Velocity from Buggy I and Peak Velocity from Scaled Almendro	4-3

1. INTRODUCTION

Under assumed provisions of a Threshold Test Ban Treaty (TTBT), the yield of a single nuclear device which could be detonated in an underground test would be limited to 150 kt or less. The terms of the assumed treaty also provide for Peaceful Nuclear Explosions (PNE) utilizing multiple nuclear detonations having a greater combined yield. It has been suggested that a party might attempt to evade the terms of an TTBT by detonating a single clandestine event having a yield greater than 150 kt in the environment of a high yield PNE. This report examines the seismic aspects of an evasion scenario. Specifically, recorded ground motion from single contained events are scaled to an appropriate yield and superimposed with the ground motion recorded from a multiple, surface cratering event detonated at the Nevada Test Site (NTS). The resulting data are then analyzed and compared to determine the observable effect of the clandestine event.

This report makes the following assumptions concerning a Threshold Test Ban Treaty:

1. The maximum yield of a single nuclear device is 150 kt.

2. Peaceful Nuclear Experiments are permitted involving simultaneous multiple explosions. The yield of each device is limited to 150 kt or less.

3. On-site scientific instrumentation is permitted for the purposes of yield estimation and seismic monitoring. The seismic instruments can be deployed anywhere within a 20 km radius of the PNE.

The above assumptions will be used to examine the constraints on the parameters associated with the clandestine event relative to the PNE.

In this report the PNE evasion scenario will be simulated using recorded ground motion from a low yield (5.5 kt) surface row-cratering event to represent the PNE. This event, Buggy I, is the

only event available (Cassity, et al., 1969) which approximates, except for yield, the conditions associated with the PNE in the evasion scenario. However, by suitably scaling the yield associated with the clandestine event relative to the yield of the PNE, the resulting simulation should reasonably represent the evasion scenario.

In Section 2, the constraints on yield, detonation delay time, and location of the clandestine event relative to the PNE are examined. In Section 3, the seismic characteristics of a multiple, surface cratering event are analyzed and compared to the seismic characteristics of a single contained event of equivalent yield. In Section 4, the superimposed seismic data are analyzed. Section 5 presents a summary and the conclusions of this study and makes recommendations for further studies.

2. EXAMINATION OF THE CONSTRAINTS ON THE YIELD, LOCATION, AND DETONATION TIME OF THE CLANDESTINE EVENT

2.1 INTRODUCTION

In order to simulate the PNE evasion scenario described in Section 1, the parameters of yield, location and detonation delay time of the clandestine event (CE) relative to the PNE must be determined. The CE parameters are constrained by both on-site and far-field scientific monitoring equipment whose function is to provide information for the detection of an evasion. The purpose of this section is to examine the constraints of the CE yield, location, and detonation delay time imposed by the monitoring instrumentation and to determine the parameters that will be used in the simulation described in Section 4. Section 2.2 deals with the question of yield while Section 2.3 considers the questions of location and detonation delay.

2.2 CONSTRAINTS ON YIELD

The evasion scenario involving a PNE and a CE can be stated as follows: a PNE consisting of n devices would be announced, each device having a yield, W, for a total PNE yield of $W_T = nW$. In order to accommodate a CE of yield W_C, the announced yield of each device in the PNE would have to be reduced by a fractional amount, f. The result would be a PNE having a modified total yield $W_T' = nfW$ and a CE having a yield $W_C = (1-f)nW$. The sum of W_T' and W_C would then equal the total yield of the announced PNE.

In order to detect a possible reduction in the total yield of the PNE, specific instrumentation (slifer devices) will be deployed to monitor the yield of each nuclear device in the PNE. All the individual yield estimates for each nuclear device will be summed and then compared with the announced total yield of the PNE. Since there is uncertainty associated with estimating yield, the fractional reduction in yield must be chosen to be compatible with the observational uncertainty in yield determination. Based on

present yield estimation capability, it appears that a reduction in yield of approximately 20 percent is reasonable so that an f = 0.8 would be appropriate.

In addition to on-site instrumentation for estimates of yield, the PNE would also be monitored by teleseismic instrumentation which also permits yield estimation. This yield determination would be for the combined yield of both the PNE and the clandestine device. Again, the yield determination will contain some uncertainty. This fact would be used to increase the yield of the clandestine device, and still operate within the yield determination uncertainty of the teleseismic information. If a 20 percent uncertainty is assumed, then multiplying the total yield by 1.2 would give a reasonable value for the combined yield of the PNE and CE. If the increased yield is associated with the CE, it is easy to show that the CE yield, W_C, would be 0.4 W_T, where W_T is the announced total yield of the PNE.

Thus, based on on-site and far-field yield estimation capability, the range on yield for the CE would be from 0.2 W_T to 0.4 W_T where W_T is the announced total yield of the PNE. The total yield of the modified PNE would be 0.8 W_T. These parameters will be used in Section 4 to determine the CE yield relative to the yield associated with the PNE.

2.3 CONSTRAINTS ON THE CLANDESTINE EVENT LOCATION AND DETONATION DELAY TIME

The terms of our assumed threshold test ban treaty also provide for the deployment of on-site seismic instruments to monitor ground motion. The amplitude and time of first arrival of seismic motion from both the PNE and CE are a direct function of the relative location and time of detonation associated with the two sources of energy. This section examines the constraints imposed on location and detonation delay time by both on-site and far-field seismic instrumentation.

Each on-site seismograph will record the sum or superposition of the ground motion caused by the PNE and the CE. For a particular seismic recording station, the peak amplitude levels of the PNE and CE wave trains are controlled by both the yields and recording distances of the two sources. The time associated with the first motion arrival from each source is controlled by the respective source-to-station distances, the wave propagation velocity in the area and by any time delay between the two detonations. Formulas for estimating the peak amplitude and first arrival time will be given below and will be then used to examine the constraints on the location of the CE relative to the PNE based on these general parameters.

For a single contained event of yield, W_c, and source-to-station distance, R_c, the expected vertical peak velocity, v_c, is given by (Environmental Research Corp., 1974)

$$v_c = 4.89\ W_c^{0.74}\ R_c^{-1.47} \qquad (2\text{-}1)$$

An empirical formula for the peak velocity associated with a multiple surface cratering event is not available. However it will be shown in Section 3, that the peak velocity from an observed multiple detonation is about a factor of 1.5 less than the peak velocity from a single contained event. Using this empirical factor, the expected peak velocity, v_p, of a PNE of combined yield, W_p, and source-to-station distance, R_p, is given by

$$v_p = 3.25\ W_p^{0.74}\ R_p^{-1.47} \qquad (2\text{-}2)$$

Also, an empirical equation is not available for estimating the peak velocity associated with the superposition of two seismic wave trains. However, a reasonable estimate can be obtained using a root-mean-square estimate given by

$$v_{pc} = \sqrt{v_p^2 + v_c^2} \qquad (2\text{-}3)$$

The equation for the time of first arrival, t_p, for a PNE with a source- to-station distance, R_p, is given by

$$t_p = \frac{R_p}{V} \qquad (2\text{-}4)$$

when V is the propagation velocity associated with P-waves. For the CE which is detonated with a time delay of Δt_c seconds, the time of first arrival, t_c, for a source-to-station distance, R_c, is given by

$$t_c = \frac{R_c}{V} + \Delta t_c \qquad (2\text{-}5)$$

In actual practice, the propagation velocity, V, would not be the same for all transmission paths, but for initial estimation purposes, a single value will be assumed.

The equations developed above will now be applied to the case in which the CE is located outside the on-site seismic array. Assume an announced PNE of 1500 kt, a modified PNE of 1200 kt and a CE of 600 kt located 40 km from the PNE. Consider two seismic stations on a line connecting the two sources, located at 10 and 20 km from the PNE. Assume also that the body wave propagation velocity is 4 km/sec and that the events are detonated simultaneously. For the station located at 10 km, the expected peak velocities and first arrival times for the individual and superimposed wave trains are as follows:

	Expected Peak Velocity	First Arrival Time
Announced PNE:	24.7 cm/sec	2.5 sec
Modified PNE:	20.9 cm/sec	2.5 sec
CE:	3.75 cm/sec	7.5 sec
Modified PNE+CE:	21.2 cm/sec	2.5 sec

These data show that the CE peak velocity would be a factor of about 5.6 below that of the PNE. The time of first arrival would appear normal. The expected peak velocity from the announced PNE and the modified PNE + CE differ by approximately 17 percent, a difference which is small compared to normal variation of observed peak velocity about the expected mean value. Thus, for the station at 10 km, the peak velocity and first arrival time from the modified PNE + CE would differ little from that expected for the announced PNE.

For the station located 20 km from both the PNE and the CE, the expected peak velocities and first arrival times are as follows:

	Expected Peak Velocity	First Arrival Time
Announced PNE	8.90 cm/sec	5 sec
Modified PNE:	7.55 cm/sec	5 sec
CE:	6.80 cm/sec	5 sec
Modified PNE+CE:	10.16 cm/sec	5 sec

In this case the peak velocities from the modified PNE and CE are nearly equal. The expected peak velocity from the modified PNE+CE is approximately 14 percent greater than that expected from the announced PNE, again an insignificant variation. In all cases the time of first arrival would be the same.

For the two cases considered above, it appears that based on the results of near-field instrumentation, the modified PNE+CE would be indistinguishable from the announced PNE and that a source separation of 40 km would be a viable evasion tactic. However, analysis of teleseismic data would lead to the conclusion that a CE had been detonated, as the following discussion will show.

Considerable effort has been expended in a program to identify two distinct sources of seismic energy based on teleseismic data. A primary factor in distinguishing two sources is the time separating T, between the initial arrivals. The time separation is a function of both the distance, ΔD, between the sources, the detonation delay time, Δt, and the distance, Δ, to the seismic recording station. The present discrimination capability is shown in Figure 2.1 (Alewine, 1978), which expresses the probability of making a specified error in classification as a function of source separation and detonation delay for recording stations at distances Δ=30° and 60°.

The information expressed in Figure 2.1 can be stated in a mathematical equation. For example, equations for Δ = 60° and for classification errors of 15 percent and 50 percent are given by

$$P(E) = 0.15; \quad 0.0625\,\Delta D + \Delta t = 2.5 \text{ sec} \tag{2-6}$$

$$P(E) = 0.50; \quad 0.0625\,\Delta D + \Delta t = 0.6 \text{ sec} \tag{2-7}$$

These equations can be considered as constraints on ΔD and Δt for the specified teleseismic detection capability.

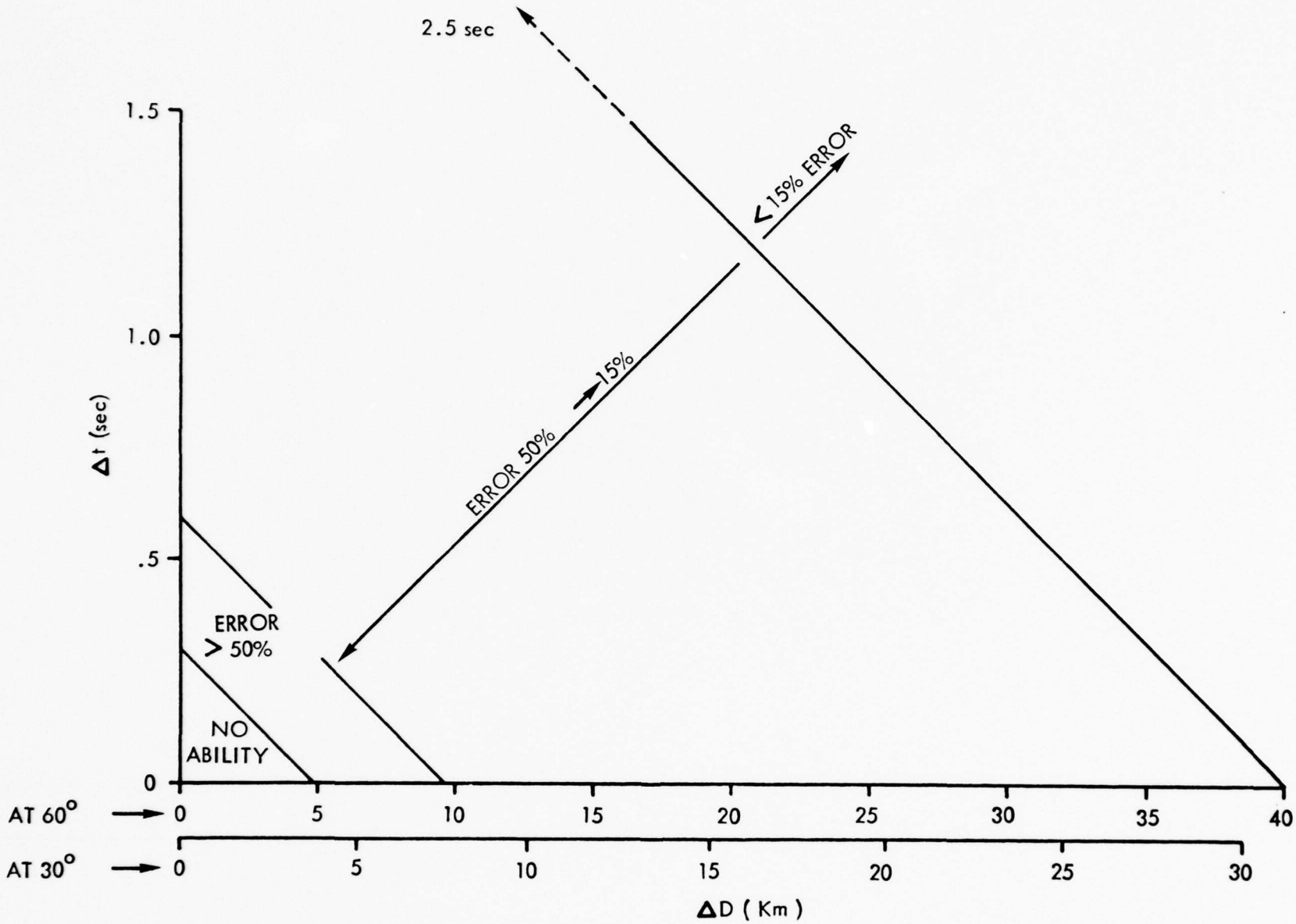

FIGURE 2.1: TELESEISMIC DISCRIMINATION OF TWO SEISMIC SOURCES BASED ON SOURCE SEPARATION, DETONATION DELAY TIME AND TELESEISMIC DISTANCE

Returning now to the PNE and CE evasion scenario in which the location separation is 40 km with zero time delay, the previous analysis, based on near-field seismic data, indicated that it would be difficult to identify the CE based on peak velocity and first arrival time. However, this case would be detectable with a 15 percent probability of error based on teleseismic information. In fact, the greater the PNE and CE source separation, the smaller the error in discriminating the two sources from teleseismic data. At the same time, the greater the difficulty in detecting the clandestine event based on on-site seismic information.

Examination of Figure 2.1 shows that as the source separation decreases, the error in discrimination capability increases for a given detonation delay. But as the source separation decreases, the clandestine event comes closer to the on-site seismic array. The consequences in terms of peak velocity and first arrival time is shown in the following example.

Assume that the source separation is 30 km and that a seismic station is located 20 km from the PNE and 10 km from the CE. Let the teleseismic discrimination error be 15 percent, so that the permissible detonation delay, is $\Delta t = 0.625$ seconds. The expected peak velocities and first arrival times at the seismic station are as follows:

	Expected Peak Velocity	First Arrival Time
Announced PNE:	8.90 cm/sec	5.0 sec
Modified PNE:	7.55 cm/sec	5.0 sec
CE:	18.84 cm/sec	3.12 sec
Modified PNE+CE:	20.29 cm/sec	3.12 sec

These data show that the expected velocity from the modified PNE+CE is more than a factor of two greater than would be expected from the announced PNE. In addition, the first arrival time would be 1.88 seconds sooner than expected. These data would certainly appear anomalous, especially the significantly smaller first arrival time.

As the source separation becomes less than 30 km, the situation becomes worse from the on-site seismic viewpoint. It seems certain that the clandestine event would not be located near possible seismic station locations. The one location for the CE which does appear feasible is directly below the PNE, i.e., zero surface separation. This location would also be desirable from a teleseismic discrimination viewpoint. If the detonation delay were restricted to 0.3 seconds or less, Figure 2.1 indicates that the probability of error in discrimination would be 50 percent or greater based on teleseismic data.

For zero separation and a 0.3 second detonation delay, the expected peak velocities and first arrival times for an on-site seismic station located at 10 km are:

	Expected Peak Velocity	First Arrival Time
Announced PNE:	24.7 cm/sec	2.5 sec
Modified PNE:	20.9 cm/sec	2.5 sec
CE:	18.89 cm/sec	2.8 sec
Modified PNE+CE:	28.1 cm/sec	2.5 sec

And for a station located at 20 km they are:

	Expected Peak Velocity	First Arrival Time
Announced PNE:	8.90 cm/sec	5.0 sec
Modified PNE:	7.55 cm/sec	5.0 sec
CE:	6.80 cm/sec	5.3 sec
Modified PNE+CE:	10.16 cm/sec	5.0 sec

The above data show that the expected peak velocity from the modified PNE+CE would be only slightly greater than expected from the announced PNE. In addition, the time of first arrival would appear normal.

Based on the above analysis, it is concluded that the most likely location for the clandestine event would be directly below the PNE. A detonation delay of 0.3 seconds or less would minimize the possibility of distinguishing the two sources of energy based on an analysis of teleseismic data.

3. COMPARISON OF A SURFACE ROW-CRATERING EVENT WITH SINGLE CONTAINED EVENTS OF EQUIVALENT YIELD

3.1 INTRODUCTION

In simulating the ground motion for a PNE evasion scenario, recorded ground motion from a single contained underground nuclear explosion will be superimposed with recorded ground motion from a multiple, surface row-cratering event representing the PNE. Because of the marked difference in the source configuration of these two classes of events, the characteristics of the seismic waves from the two types of sources should also be different. This section examines quantitative differences in peak amplitude and spectral characteristics of ground motion from these two classes of events. In addition, this section describes the available seismic data sample that will be used in the simulated PNE evasion scenario.

3.2 THE SURFACE ROW-CRATERING EVENT

On March 12, 1968, a plowshare experiment, Buggy I, was conducted at the Nevada Test Site and involved the near surface detonation of five nuclear devices with a combined yield of 5.5 kt (Cassity, et al., 1969). The nuclear devices had yields of 1.1 kt and were buried at a depth of 135 ft. The devices were in-line with a horizontal spacing of 135 ft. which gives a 600-foot spacing between the end devices. Buggy I is the only surface row-cratering event for which seismic recordings are available.

The available seismic data from the Buggy I event consists of the vertical component of ground velocity recorded at four stations. The stations are designated as 447, 458, 449, and 450 and are located, respectively, at surface distances of 2.69, 2.98, 6.37, and 11.1 km from the center of the Buggy I configuration. The relationship of each seismic station to Buggy I is given in Figure 3.1 which shows three stations in-line and one station at 135° relative to the direction defined by the nuclear devices.

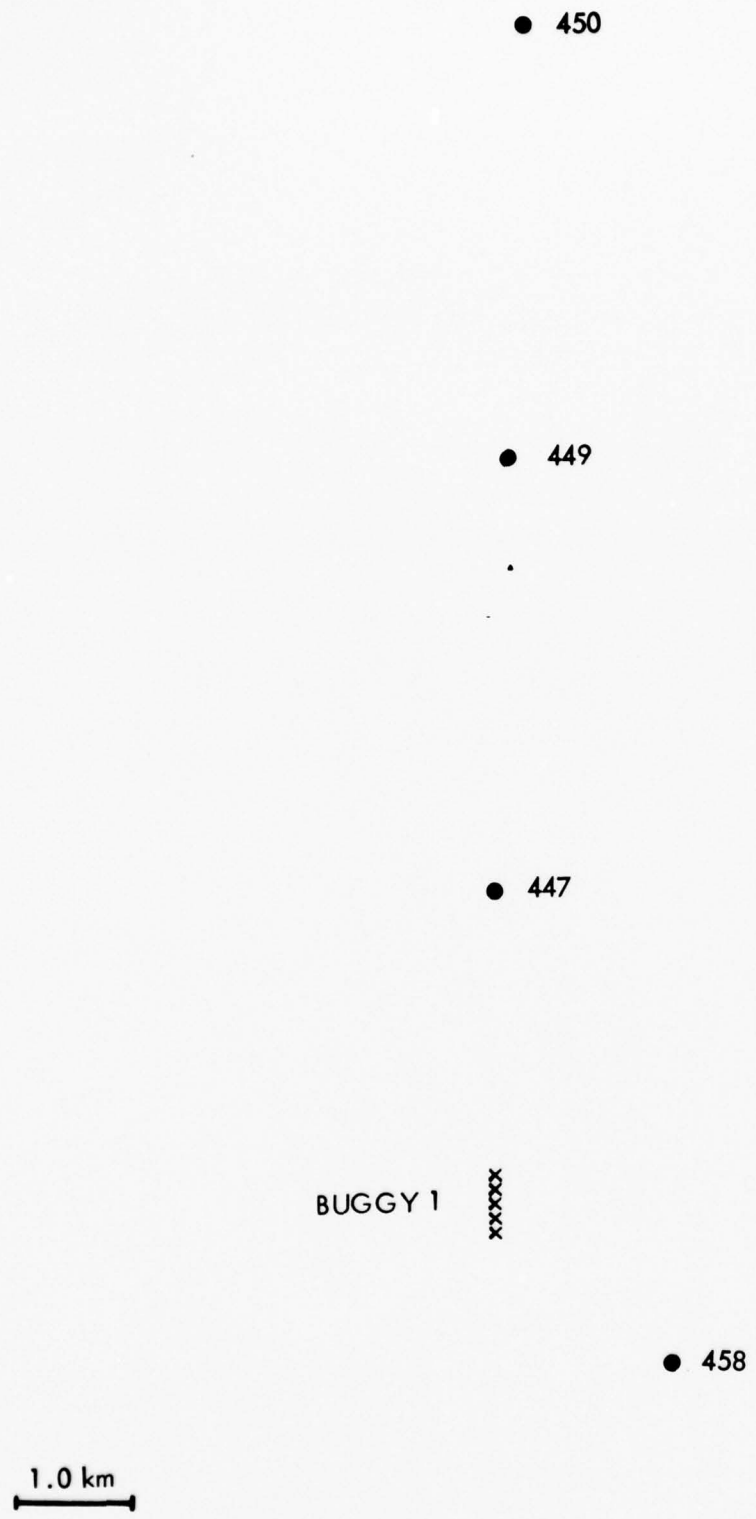

FIGURE 3.1: THE LOCATION OF THE SEISMIC RECORDING STATIONS RELATIVE TO THE BUGGY I EVENT

The observed motion from Buggy I will be used as the PNE in the evasion scenario. In Section 2, it was shown that the yield of the CE could range between 20% to 40% of the announced PNE yield and still fall within the yield determination uncertainty of both on-site and far-field instrumentation. For the Buggy I total yield of 5.5 kt, which would be the modified PNE yield or 80% of the announced PNE yield, the yield association with the announced PNE would be 5.5 kt/0.8 = 6.875 kt. The yield range association with the CE would be 20% to 40% of the announced PNE yield or a yield range of 1.375 kt to 2.75 kt. In Section 4, simulations will be performed for two cases for the CE yield. The actual yield values used are 1.375 kt and 2.5 kt.

3.3 SINGLE CONTAINED EVENTS

A search of the available data bank of NTS seismograms revealed a sample of 26 vertical velocity recordings at stations within 12 km of the detonation point. Within this set, 11 matched the source-to-station distances associated with the Buggy I event. None of the events associated with the velocity seismograms had yields of 1.375 or 2.5 kt that are required for the PNE evasion simulation.

Fortunately, procedures have been developed to scale observed seismogram time histories for the source parameters of yield and depth of burial (Mueller and Murphy, 1971; Murphy, 1977). Essentially, an observed time history is operated on by a frequency-dependent transfer function containing, as parameters, the actual and desired yield and depth of burial. The result is an estimated time history scaled to the desired yield and depth of burial. Examples of transformed seismograms are given in Murphy, 1977.

3.4 COMPARISON OF THE SEISMIC CHARACTERISTICS OF A SURFACE ROW-CRATERING AND SINGLE CONTAINED EVENTS OF EQUIVALENT YIELD

The seismic characteristics of time histories from single contained events detonated at the NTS have been extensively studied since the beginning of the underground nuclear testing program. Based on analyses of observed data, empirical equations have been developed to estimate the peak amplitude and spectral amplitude of ground motion as a function of the yield of the device and the source-to-station distance. Because of the limited experience with surface row-cratering events, amplitude and spectral scaling relationships are unknown. The purpose of this section is to compare the peak amplitude and spectral characteristics of Buggy I seismograms with those characteristics obtained from a set of close-in seismograms from single contained events scaled to the equivalent yield.

The peak velocities from single contained events scaled to 5.5 kt have been analyzed statistically using a power law relationship given by

$$v_p = v_0 R^{-n} \tag{3-1}$$

where v_p and R are observations and v_0 and n are constants to be determined. An analysis results in the equation

$$\hat{v}_p = 10.9R^{-1.67} \tag{3-2}$$

where $\hat{v}_p$ is the expected peak velocity in cm/sec and the source-to-station distance, R, is in km. The statistical analysis also gives an estimate of the scatter of the observations about the expected value. This measure of scatter is called the standard error of estimate, σ, and the analysis gives $\sigma = 2.1$. Multiplying and dividing the expected peak velocity, $\hat{v}_p$, by defines an interval in which 67% of the observations are expected to fall.

A plot of equation 3.1 together with the observed peak velocities from the scaled single contained events and the observed peak velocities from Buggy I are shown in Figure 3.2. As this figure indicates, the peak velocities from Buggy I fall below the line defining the expected peak velocity. On the average, the Buggy I peaks are a factor of 1.5 below the expected value for a single contained event of equivalent yield. Figure 3.2 also shows the considerable scatter associated with observed peak velocities. In addition to peak velocity, the single contained events have been analyzed to determine spectral information using a narrow-band filter technique. The filters utilized in the analysis are second order active filters characterized by a center frequency, f_i, and a damping factor, h, which was chosen to be 5 percent of critical damping. The transfer function, F(S), of this filter is given by

$$F(S) = \frac{2hw_i^2}{S^2 + 2hw_iS + w_i^2} \qquad (3\text{-}3)$$

where S is the Laplace transform variable, and $w_i = 2\pi f_i$. Each seismogram is processed through a set of narrow-band filters each having a different center frequency. The peak amplitude response from each filter represents the spectral value S_{vi} for each center frequency, f_i. It is customary to plot, S_{vi}, versus period, p_i, which is related to frequency by $p_i = 1/f_i$. An example of the spectral information obtained using this technique is shown in Figure 3.3.

As was done with peak velocity, spectral information was analyzed statistically using a power law given by

$$S_{vi} = S_{voi}R^{-ni} \qquad i = 1, 2...N. \qquad (3\text{-}4)$$

where S_{vi} and R are observed and S_{voi} and n_i are parameters to be estimated for each period, p_i. The analysis results which give estimates of S_{voi}, n_i and the standard error of estimate, s_i, are shown in Table 3.1

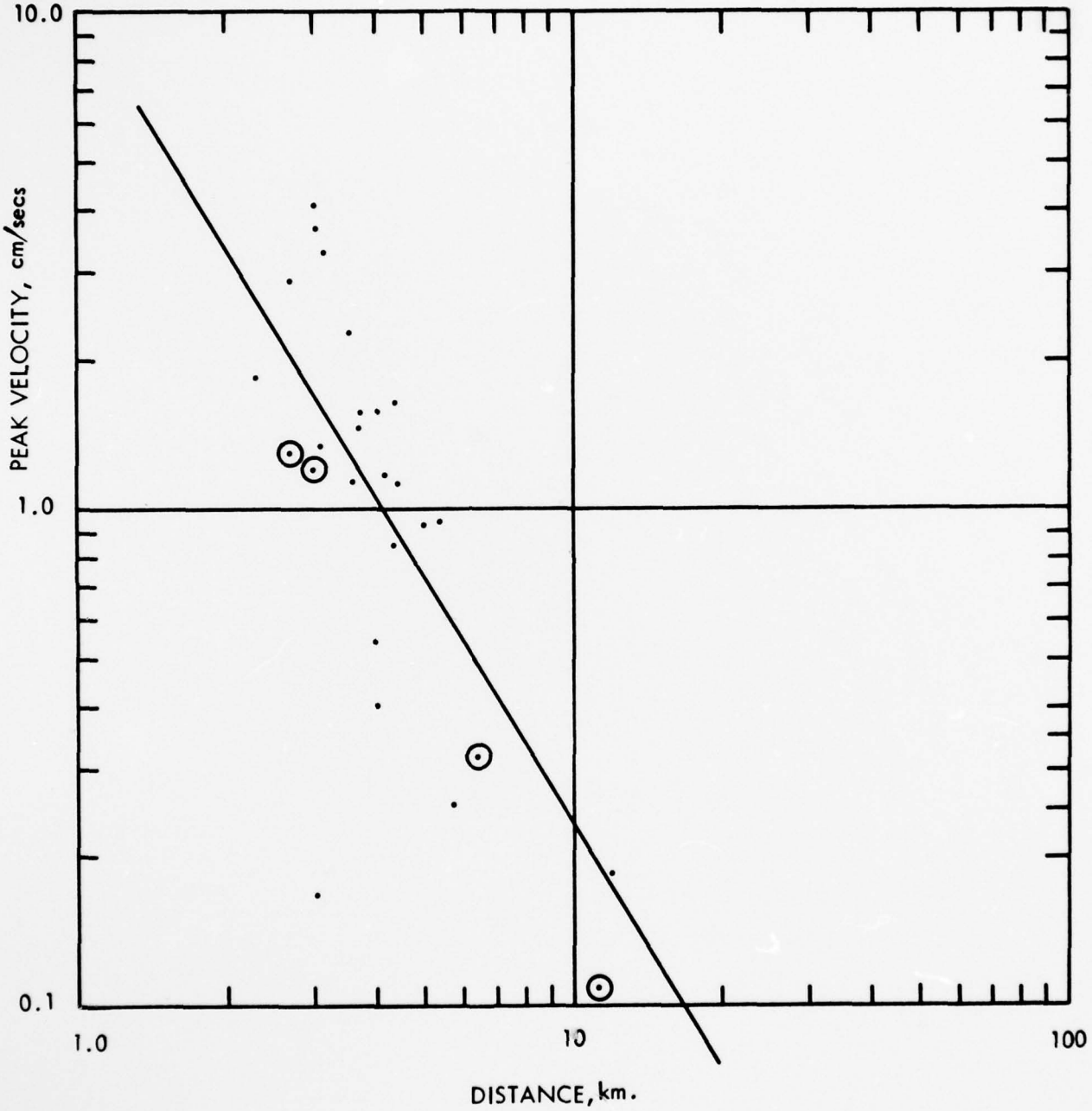

FIGURE 3.2: A PLOT OF THE PEAK VELOCITY VERSUS DISTANCE FOR BUGGY I (CIRCLES) AND SINGLE CONTAINED EVENTS (DOTS)

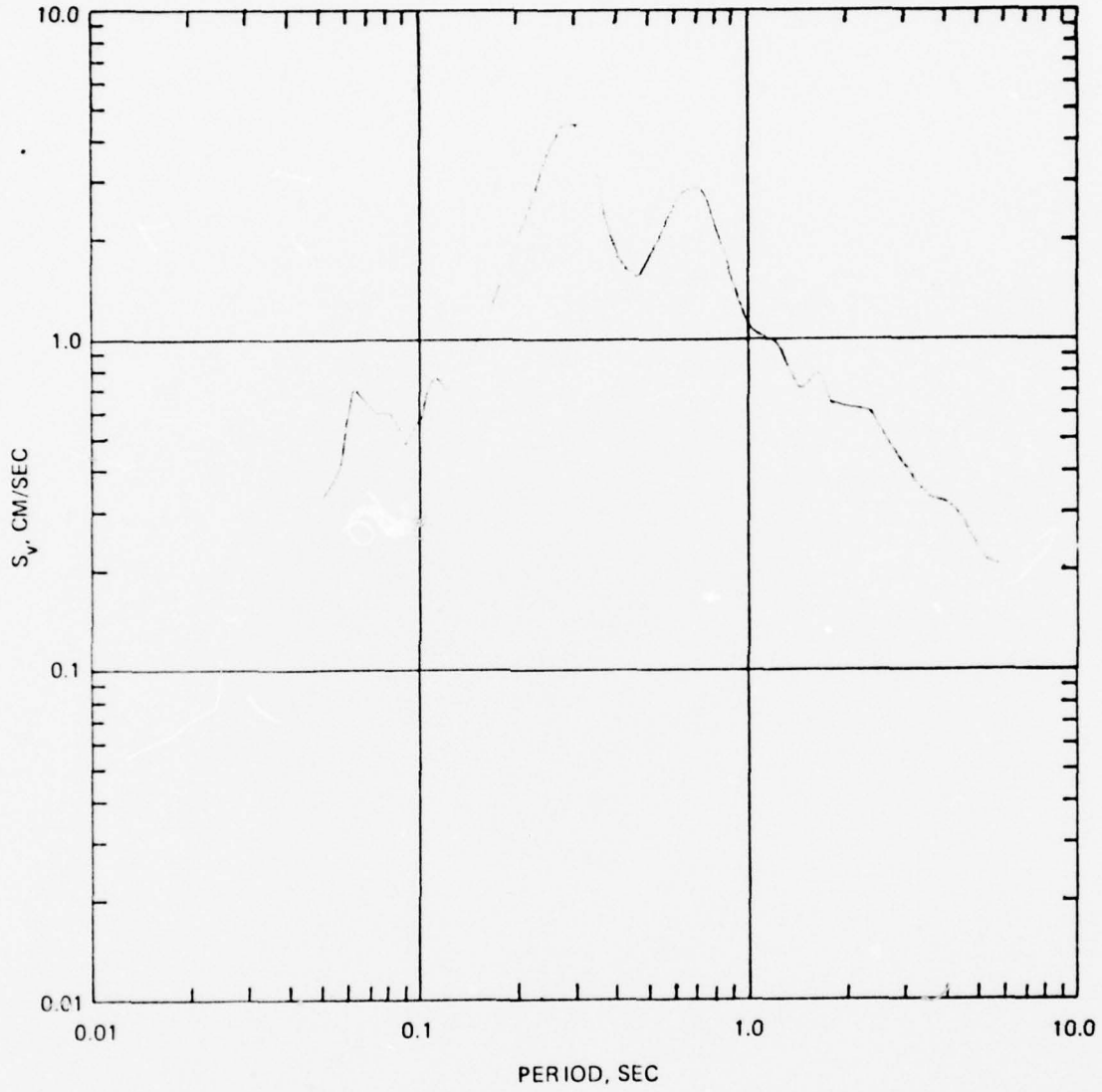

FIGURE 3.3: AN EXAMPLE OF AN AMPLITUDE SPECTRA OBTAINED USING THE NARROW-BAND FILTER TECHNIQUE

A plot of the expected spectral value for the period 0.499 seconds is shown in Figure 3.4 together with the observed spectral values from single contained events and from the Buggy I event. These data show that the spectral values from Buggy I are all lower than that expected from a single contained event. The average ratio of expected to observed Buggy I is 2.5 at this period. The average ratios for the 13 periods examined are shown in Figure 3.5. At all but one period, the ratio is greater than one.

In terms of both peak amplitude and spectral values, single contained events can be expected to give greater amplitudes than a surface row-cratering event of equivalent yield.

Section 3 has examined the differences in peak amplitude and the spectral characteristics of the Buggy I surface row-cratering event and single contained events of equivalent yield. In Section 4, ground motion from these two classes of events will be superimposed to simulate the PNE evasion scenario and will be analyzed to determine the effects caused by the clandestine event.

TABLE 3.1

ESTIMATED PARAMETER FROM THE ANALYSIS
OF SPECTRAL INFORMATION FROM SINGLE, CONTAINED EVENTS

Period	S_{vo}	m	σ_s
0.050	2.95	2.03	2.19
0.067	3.98	1.95	2.22
0.100	9.54	2.13	2.21
0.150	26.0	2.48	2.13
0.224	52.8	2.58	2.33
0.334	29.1	1.72	2.21
0.499	25.2	1.58	2.13
0.743	18.67	1.58	2.49
1.110	12.83	1.48	2.72
1.650	3.90	0.98	2.46
2.470	1.10	0.72	2.18
3.680	1.368	1.26	2.71
6.070	.182	0.135	2.35

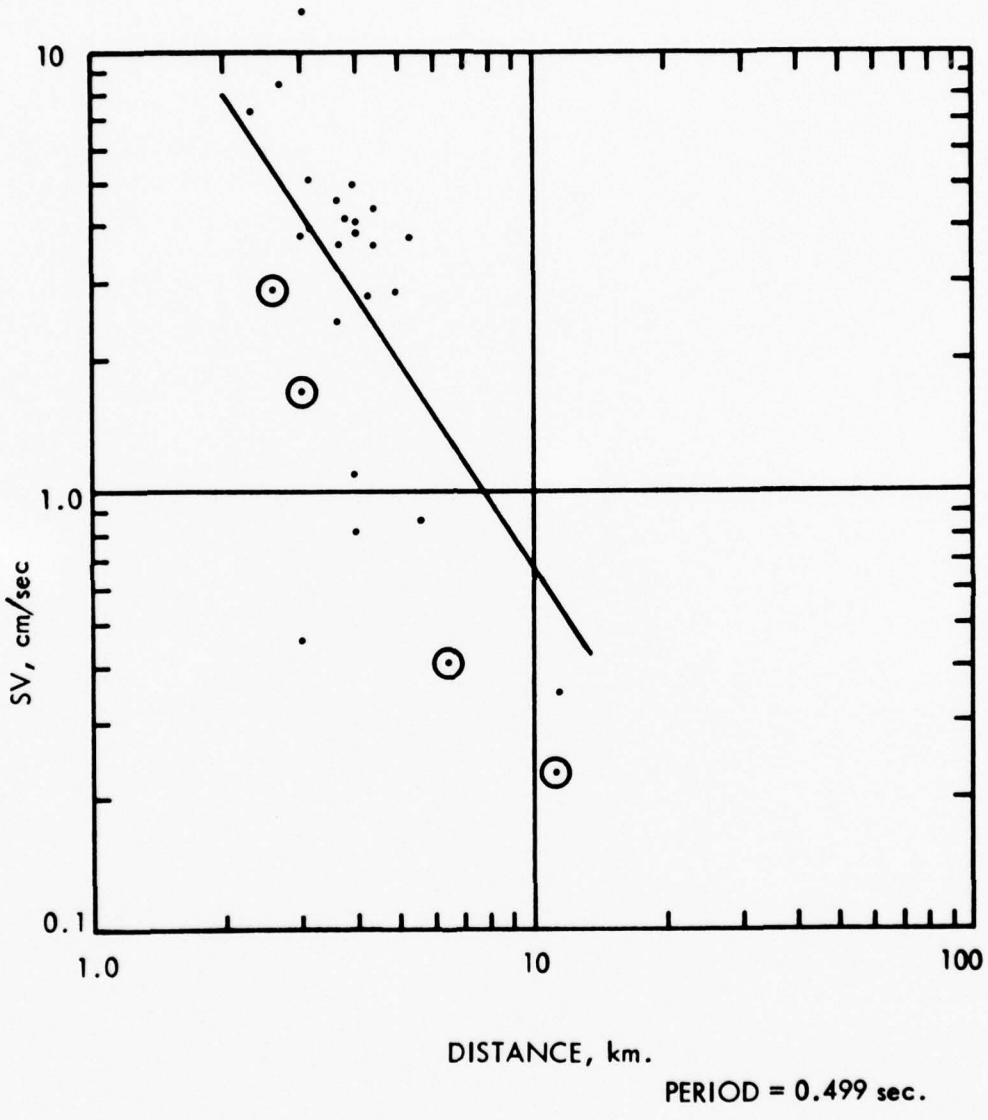

FIGURE 3.4: SPECTRAL AMPLITUDE VERSUS DISTANCE FOR BUGGY I (CIRCLES) AND SINGLE CONTAINED EVENTS (DOTS)

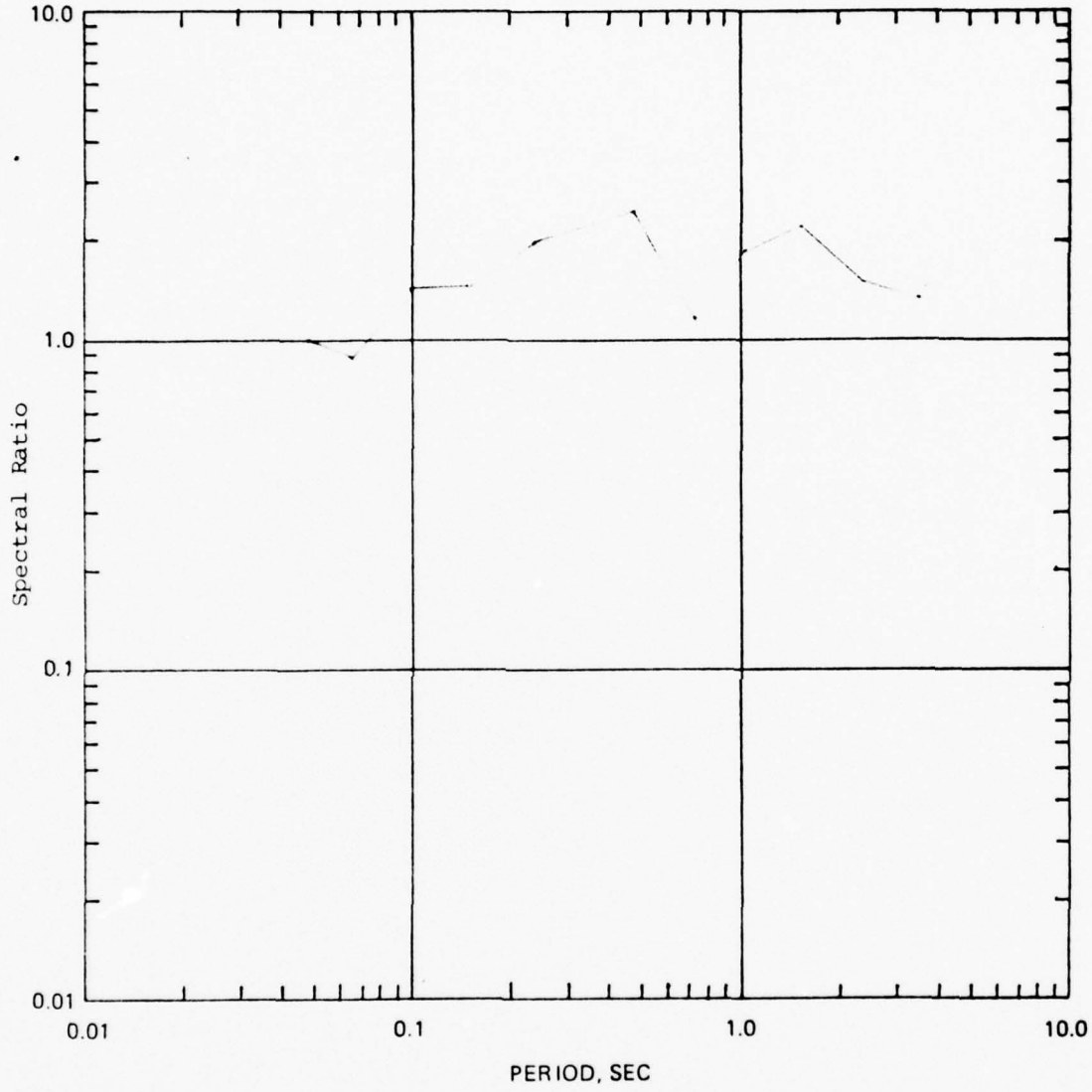

FIGURE 3.5: A PLOT FOR THE AVERAGE SPECTRAL RATIO OF SINGLE CONTAINED EVENTS TO BUGGY I

4. SIMULATION AND ANALYSIS OF THE PNE EVASION SCENARIO

4.1 INTRODUCTION

The purpose of this section is to present the results of a simulated PNE evasion scenario using observed seismograms from the Buggy I row-cratering events and single contained events scaled to two simulation yields: 1.375 kt and 2.5 kt. Seismograms from these two classes of events are summed using a time delay of 0.3 seconds. Spectral content of the Buggy I seismograms will be compared to the spectral content of the superposition.

4.2 DATA SAMPLE

Seismograms from the single contained event data sample were selected on the basis of the source-to-station distances associated with Buggy I. General information concerning the selected events is given in Table 4.1 which identifies each event and station associated with the Buggy I stations and provides information on the yield and distance for the single continued events. Seven of the 13 seismograms are associated with the Almendro event which has the highest yield in the sample. Almendro stations L03 and L04 are used to form superpositions with Buggy I stations 447 and 458, even though the source-to-station distances are only approximately the same.

Each of the single contained event seismograms was scaled to the CE yields of 1.375 and 2.5 kt using the source scaling technique referenced in Section 3. The data were checked for reasonableness by comparing the peak velocity of the scaled seismograms with the peak velocity associated with Buggy I. Examination of these data indicated unreasonably large peak velocities for some Almendro stations. This can be seen in Table 4.2 which gives the peak velocities of all the Buggy I stations and the 1.375 kt scaled Almendro

TABLE 4.1

GENERAL EVENT INFORMATION

Buggy I(5.5kt)	
Station	Distance
447	2.69
458	2.97
449	6.37
450	11.1

Single Contained Events			
Event	Station	Distance (km)	Yield Classification*
A	790	2.73	L
Almendro	L03	3.00	I
Almendro	L04	3.04	I
A	750	3.09	L
A	780	3.04	L
B	L08	3.01	L-I
Almendro	L03	3.00	I
C	765	5.70	L
Almendro	L05	5.00	I
Almendro	L02	6.03	I
Almendro	A19T	6.50	I
D	CPI	11.9	L-I
Almendro	L06	10.1	I

* L = Low yield: 0 to 20 kt.

L-I = Low-intermediate yield: 20 to 200 kt.

I = Intermediate yield: 200 kt to 1 Mt.

TABLE 4.2

OBSERVED PEAK VELOCITY FROM BUGGY I
AND PEAK VELOCITY FROM SCALED ALMENDRO

Buggy I			Scaled Almendro (1.375 kt)		
Station	Distance (km)	Peak Velocity (cm/sec)	Station	Distance (km)	Peak Velocity (cm/sec)
447	2.69	1.30	L03	3.00	0.69
			L04	3.04	0.97
458	2.97	1.20	L03	3.00	0.69
			L04	3.04	0.97
449	6.37	0.32	L05	5.0	0.52
			L02	6.03	1.12
			A19T	6.50	1.36
450	11.1	0.11	L06	12.1	0.32

stations. Almendro stations L02 and A19T are respectively a factor of 3.5 and 4.25 greater than the observed Buggy I peak velocity at station 449. Because of the large yield extrapolation involved in the source scaling, >200 to 1.375 kt, these data may be questionable. Therefore, an amplitude adjustment factor was applied to the scaled Almendro seismograms so that the ratio of observer Buggy I to scaled Almendro agreed with what would be prediction based on the peak amplitude prediction equations.

4.3 SUPERPOSITION OF SCALED ALMENDRO AND BUGGY I

Using the 0.3-second time delay, the scaled single contained Almendro event seismograms were added to the appropriate Buggy I seismograms to form the superposition seismograms. Examples showing each individual seismogram and the superposition are given in Figures 4.1 through 4.8. The amplitude scale is the same for each seismogram in a given figure. Examination of these figures indicates that the scaled Almendro seismograms are relatively short transient waveforms in comparison to the Buggy I seismograms; consequently, the superposition seismograms differ primarily in the front part of the record.

Spectra from both Buggy I and the superposition seismograms were generated and are shown in Figures 4.9 through 4.16 for clandestine event yields of 1.375 and 2.5 kt. These data show that, for periods greater than 0.6 seconds, the Buggy I and the superposition spectra are very nearly equal at all stations. For periods shorter than 0.6 seconds, the superposition spectra are, in general, greater than the Buggy I spectra.

Spectral ratios were computed and then geometrically averaged to define quantitatively the difference between Buggy I and the superpositions. The result are shown in Figure 4.17 for the two yields used in scaling the Almendro data. The maximum ratio occurs at 0.1 seconds (10 Hz).

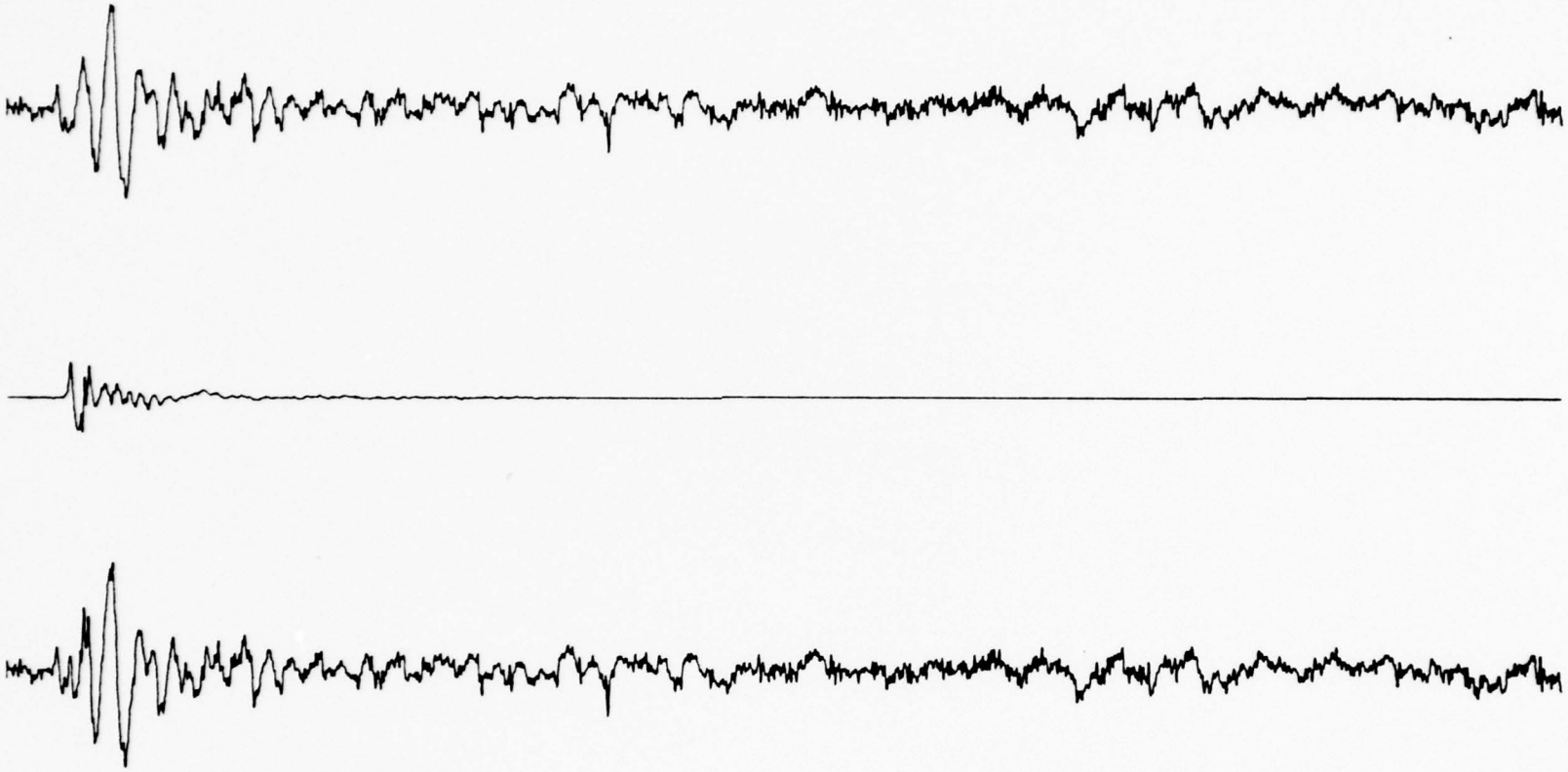

FIGURE 4.1: SEISMOGRAMS FROM BUGGY I, STATION 447 (Top Trace); SCALED ALMENDRO (1.375 kt), STATION L03 (Middle Trace); AND THE SUPERPOSITION (Bottom Trace)

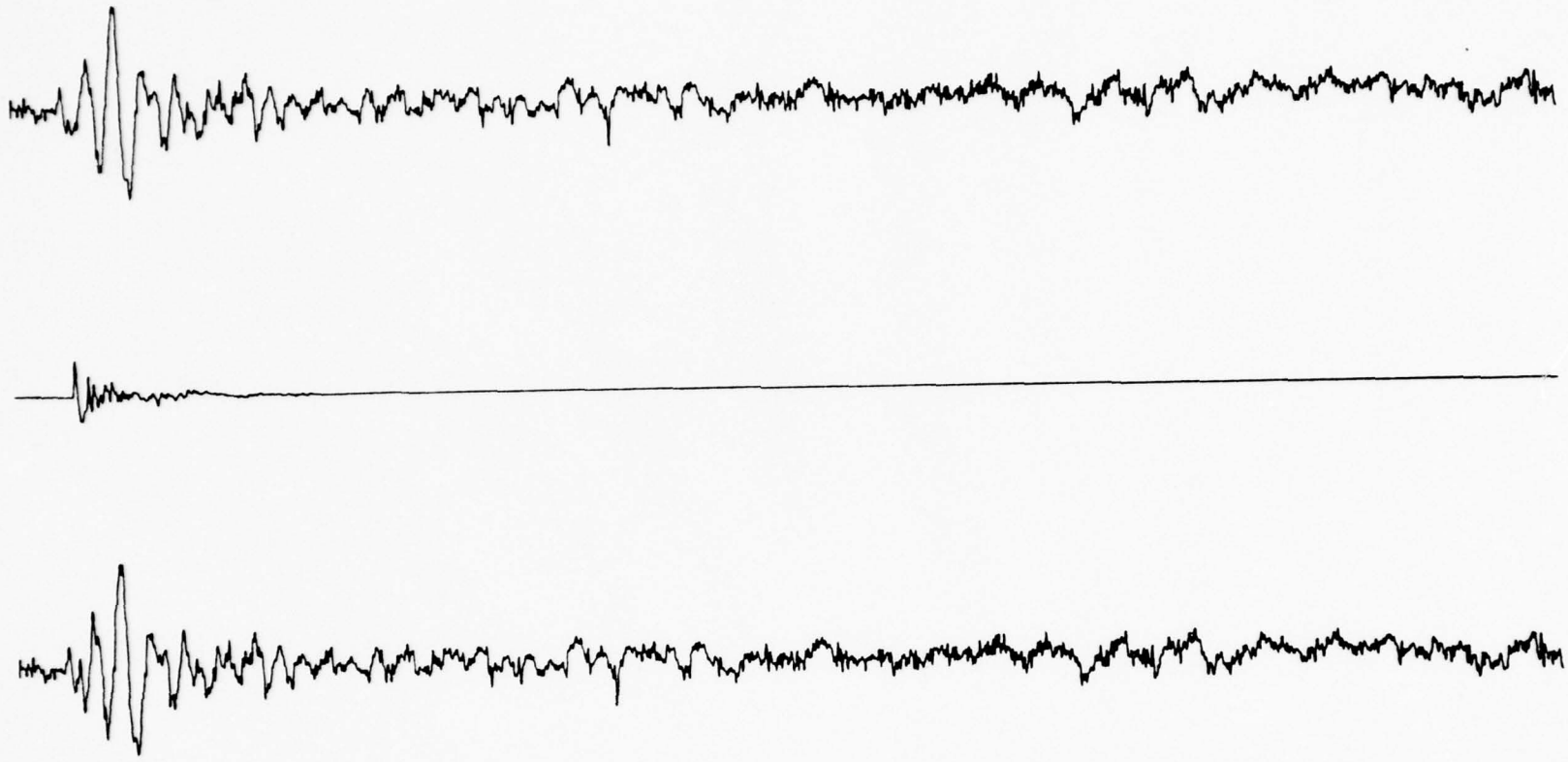

FIGURE 4.2: SEISMOGRAMS FROM BUGGY I, STATION 447 (Top Trace); SCALED ALMENDRO (1.375 kt), STATION L04 (Middle Trace); AND THE SUPERPOSITION (Bottom Trace)

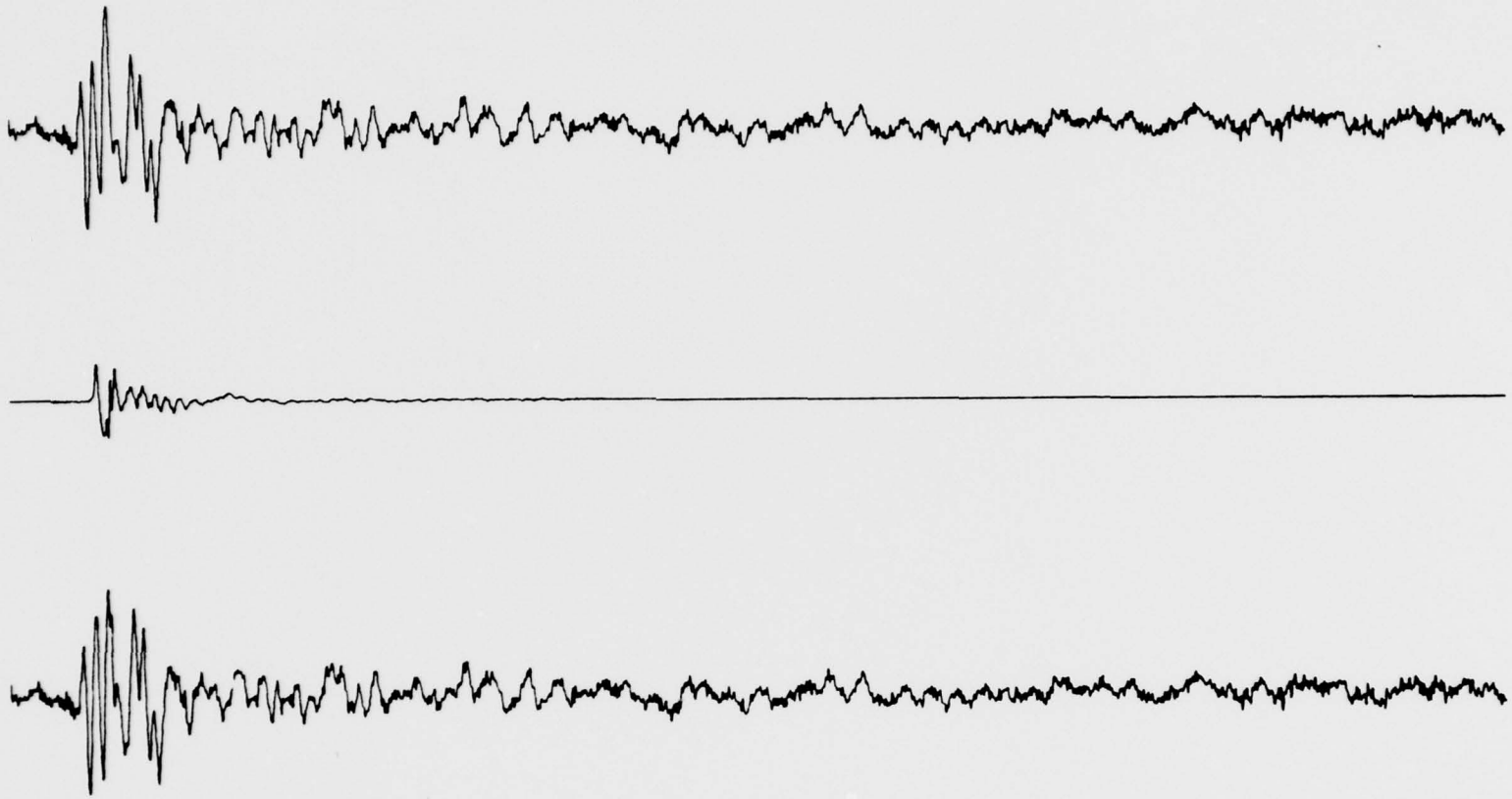

FIGURE 4.3: SEISMOGRAMS FROM BUGGY I, STATION 458 (Top Trace); SCALED ALMENDRO (1.375 kt), STATION L03 (Middle Trace); AND THE SUPERPOSITION (Bottom Trace)

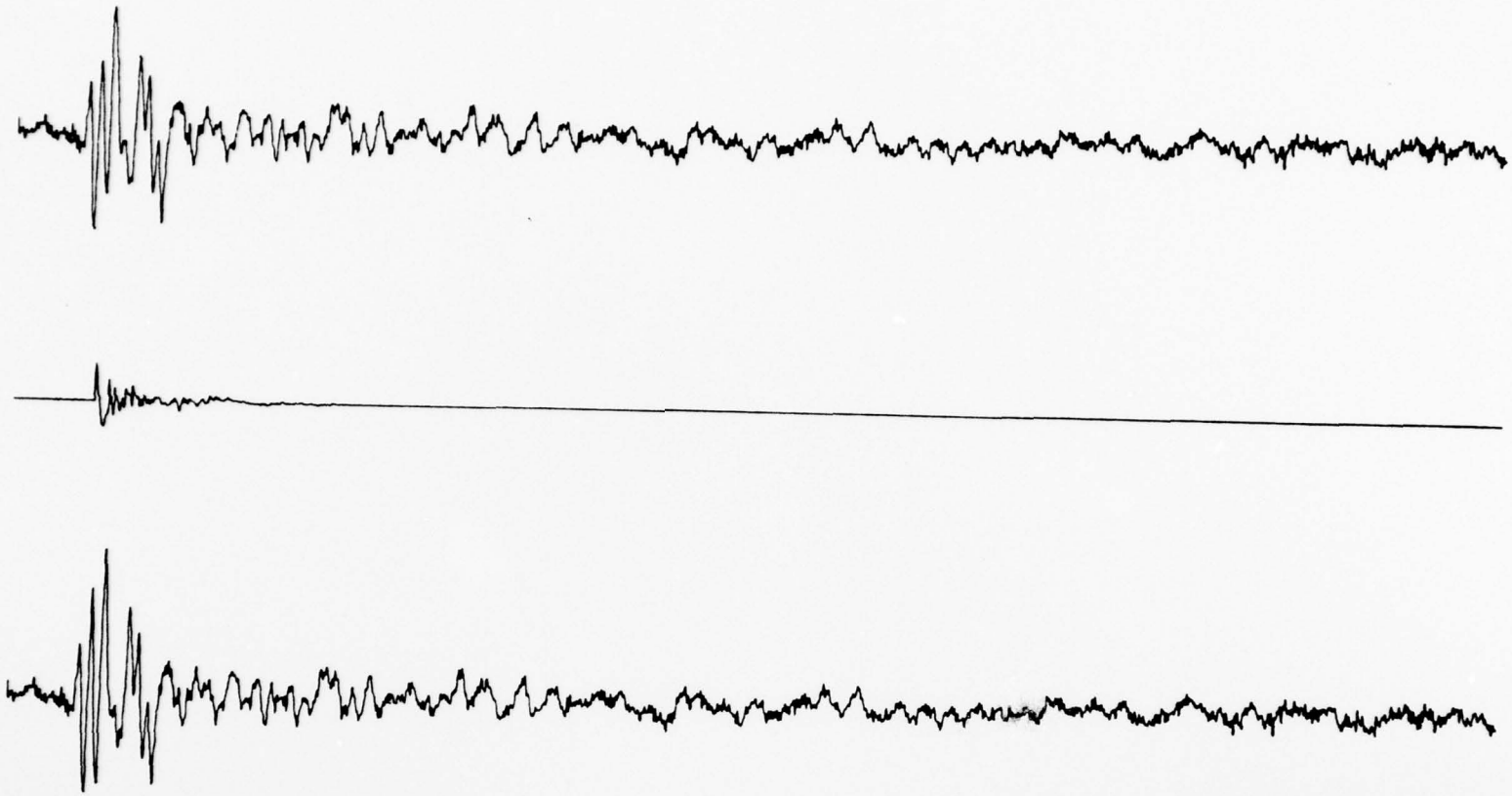

FIGURE 4.4: SEISMOGRAMS FROM BUGGY I, STATION 458 (Top Trace); SCALED ALMENDRO (1.375 kt), STATION L04 (Middle Trace); AND SUPERPOSITION (Bottom Trace)

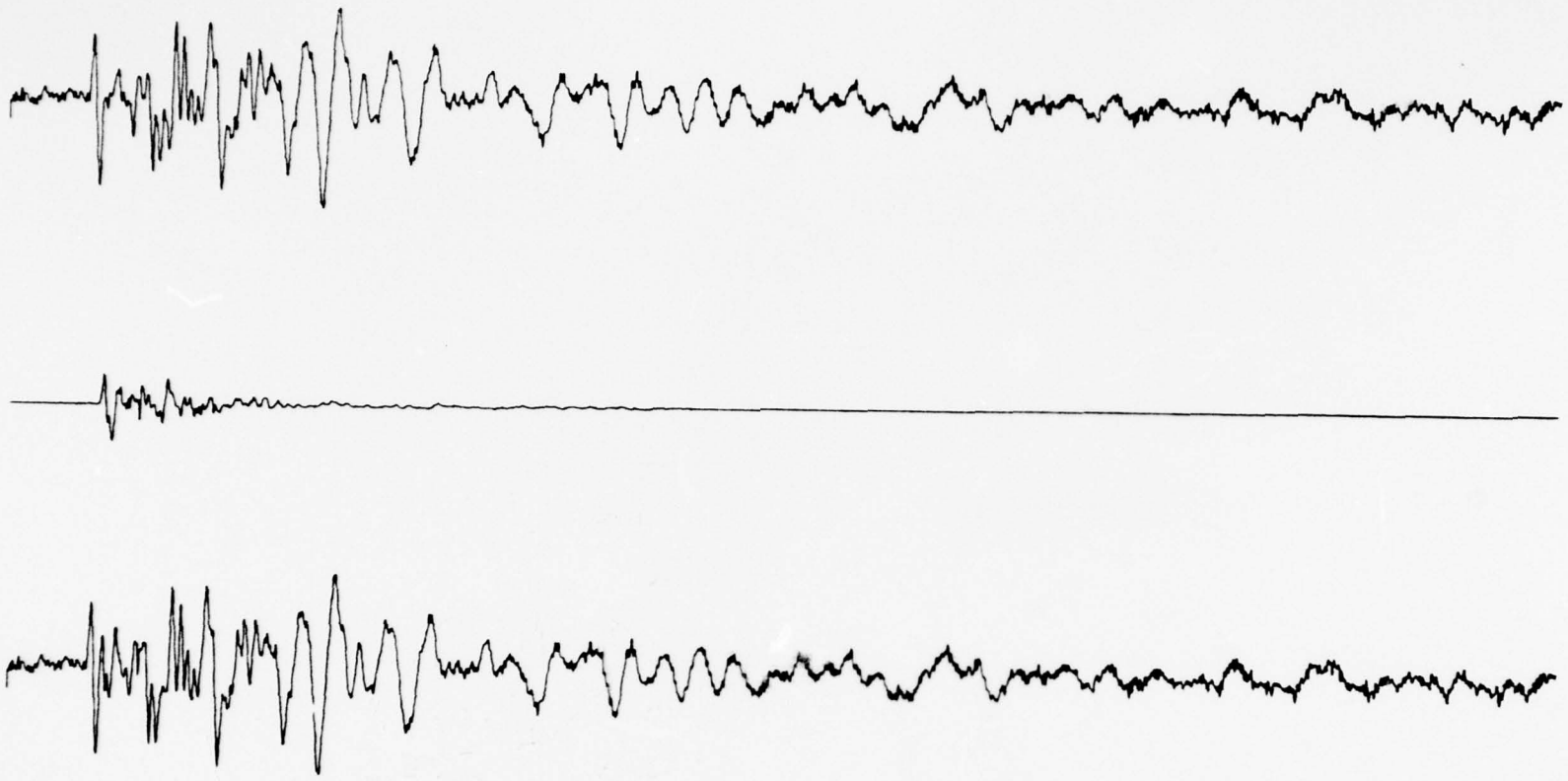

FIGURE 4.5: SEISMOGRAMS FROM BUGGY I, STATION 449 (Top Trace);SCALED ALMENDRO (1.375 kt); STATION L05 (Middle Trace); AND THE SUPERPOSITION (Bottom Trace)

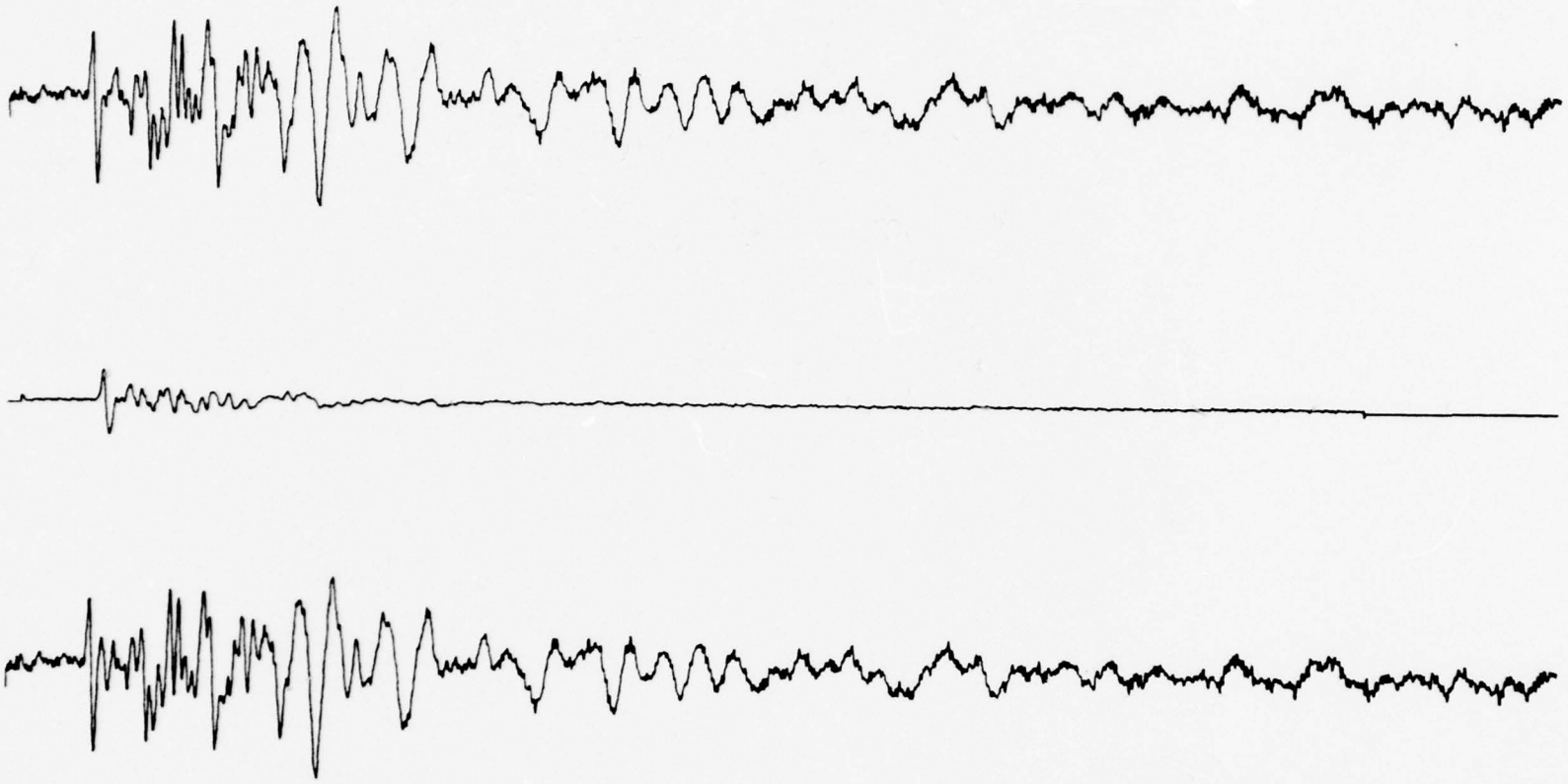

FIGURE 4.6: SEISMOGRAMS FROM BUGGY I, STATION 449 (Top Trace); SCALED ALMENDRO (1.375 kt); STATION L02 (Middle Trace); AND THE SUPERPOSITION (Bottom Trace)

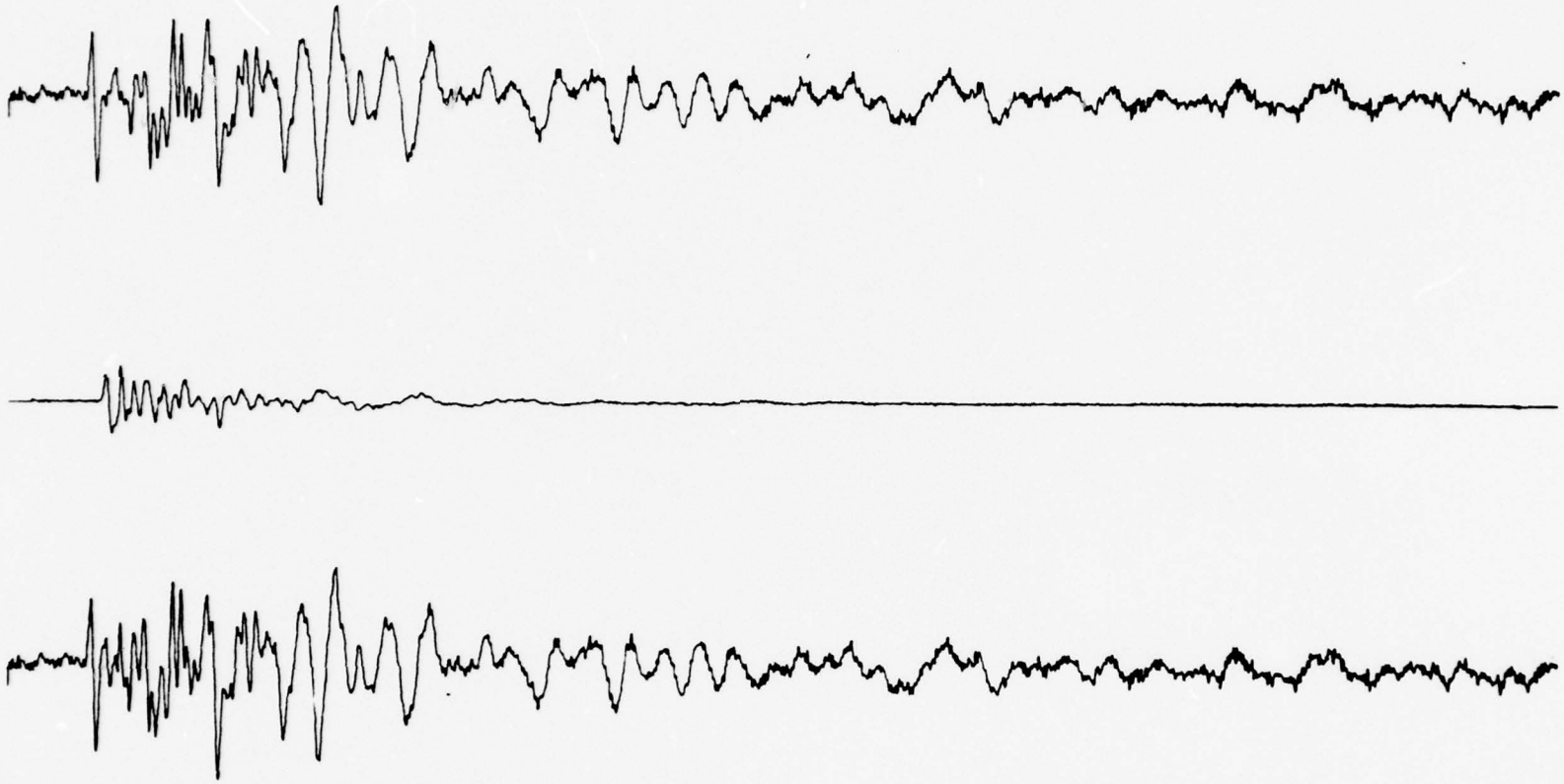

FIGURE 4.7: SEISMOGRAMS FROM BUGGY I, STATION 449 (Top Trace); SCALED ALMENDRO (1.375 kt); STATION A19T (Middle Trace); AND THE SUPERPOSITION (Bottom Trace)

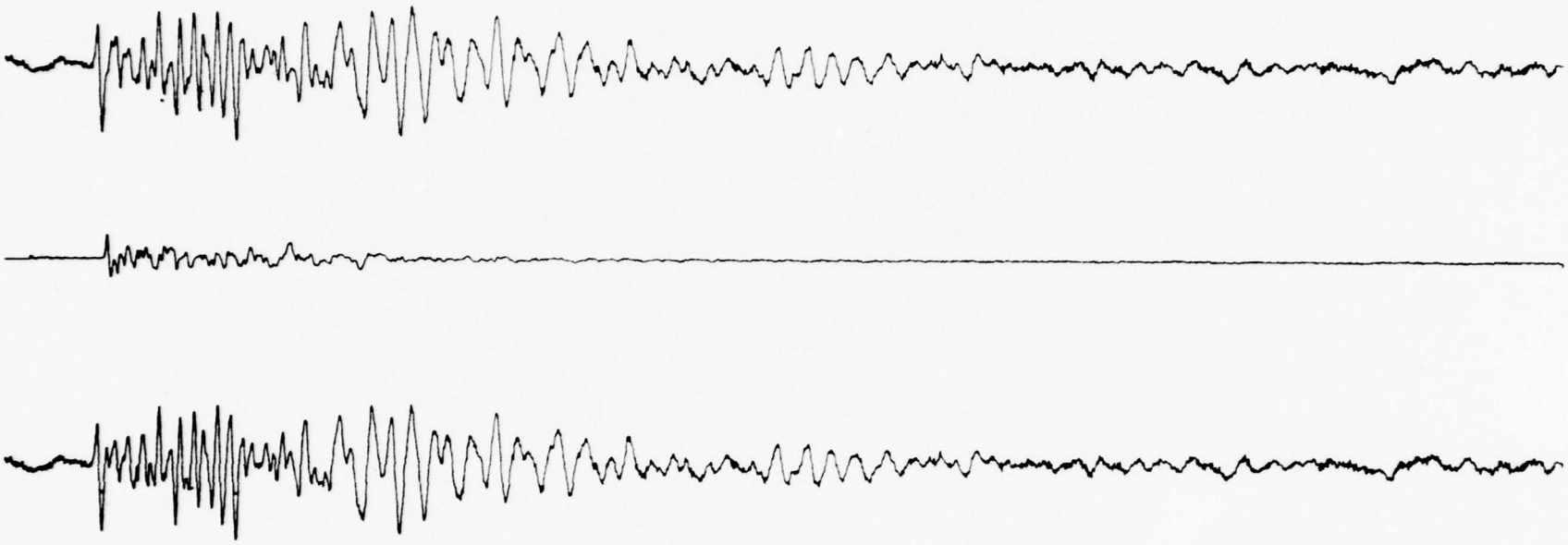

FIGURE 4.8: SEISMOGRAMS FROM BUGGY I, STATION 450 (Top Trace); SCALED ALMENDRO (1.375 kt) STATION L06 (Middle Trace); AND THE SUPERPOSITION (Bottom Trace)

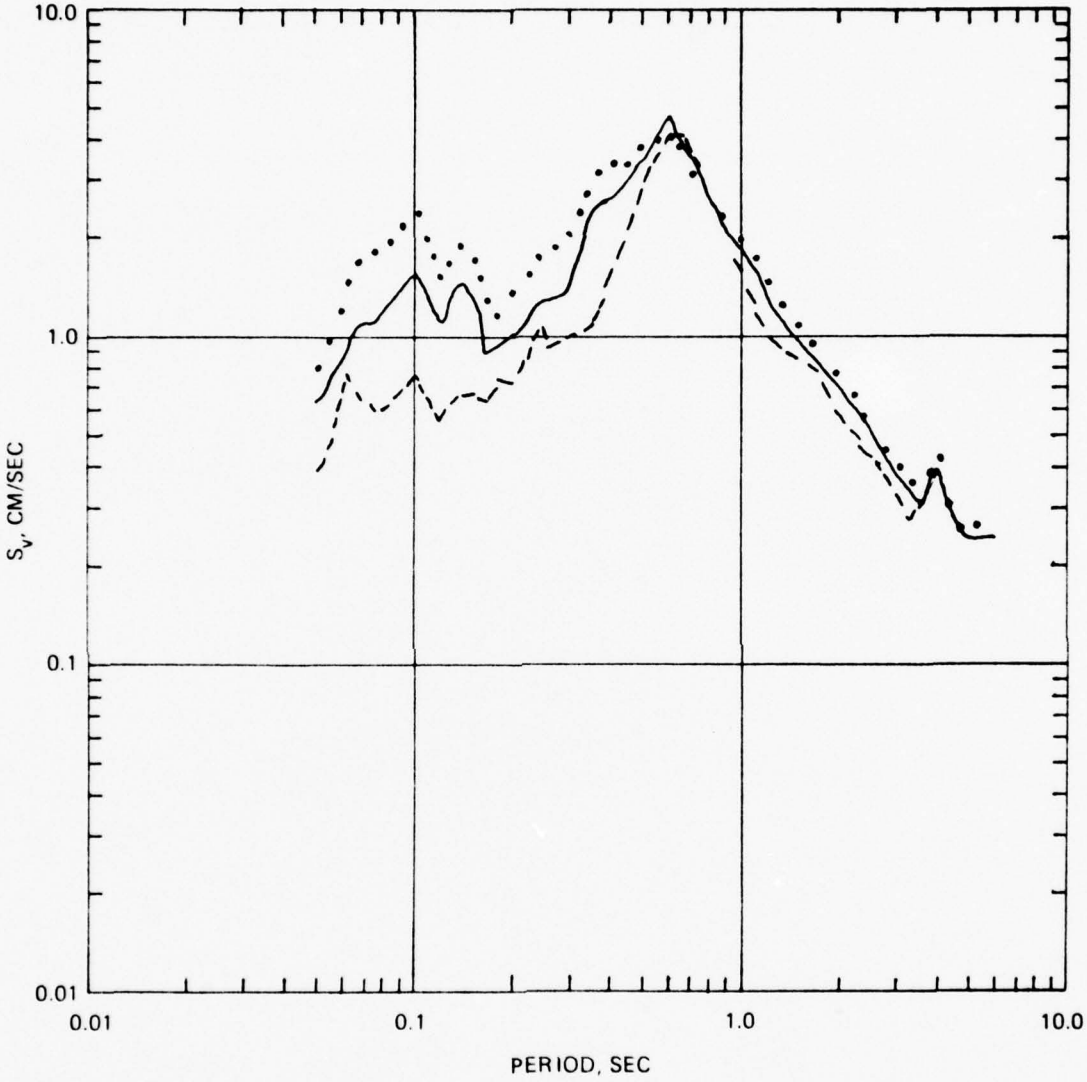

FIGURE 4.9: SPECTRA FROM BUGGY I, STATION 447 (DASHED CURVE) AND THE SUPERPOSITION WITH SCALED ALMENDRO, STATION L03, 1.375 kt (SOLID CURVE) AND 2.5 kt (DOTTED LINE)

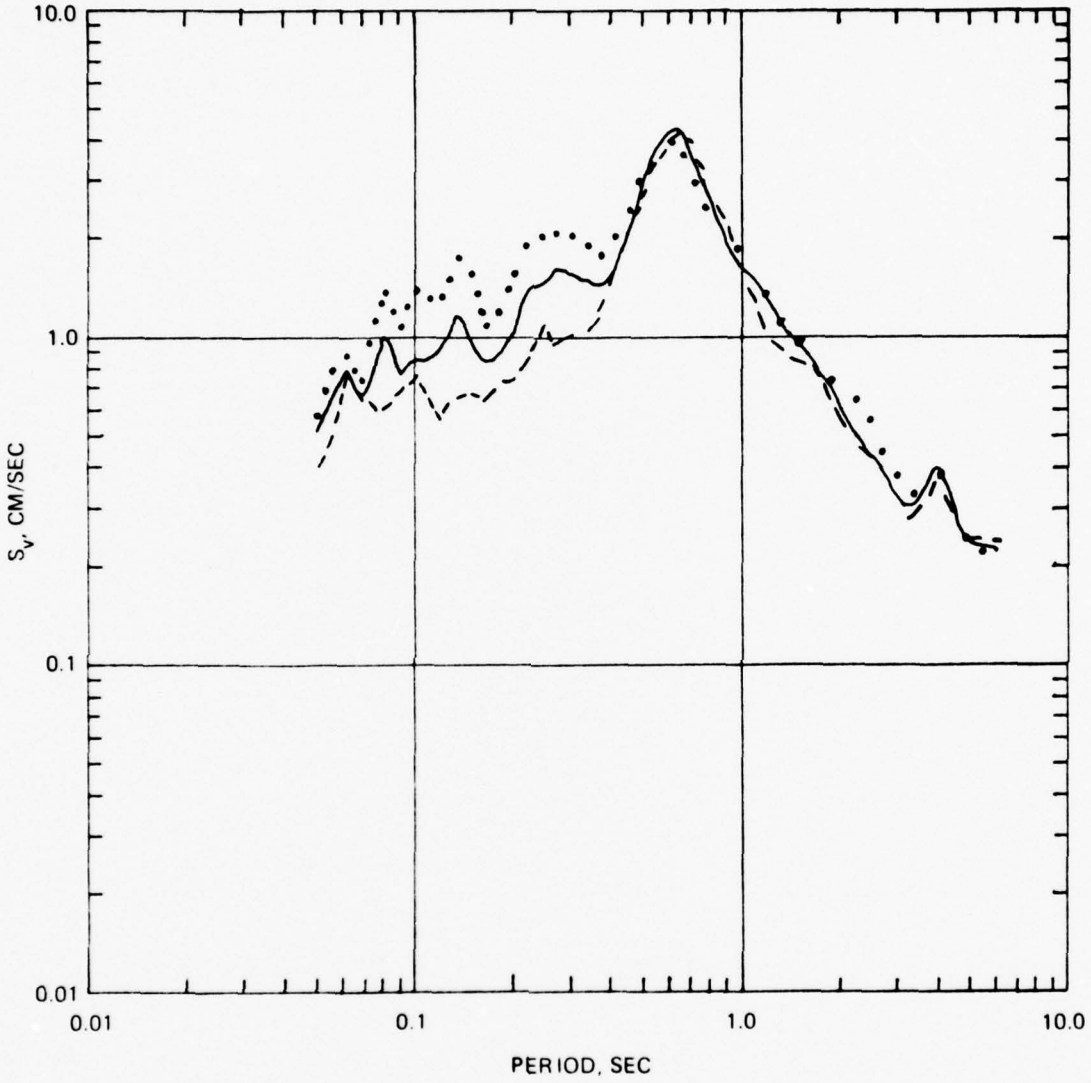

FIGURE 4.10: SPECTRA FROM BUGGY I, STATION 447 (DASHED CURVE) AND THE SUPERPOSITION WITH SCALED ALMENDRO, STATION L04, 1.375 kt (SOLID CURVE) AND 2.5 kt (DOTTED CURVE)

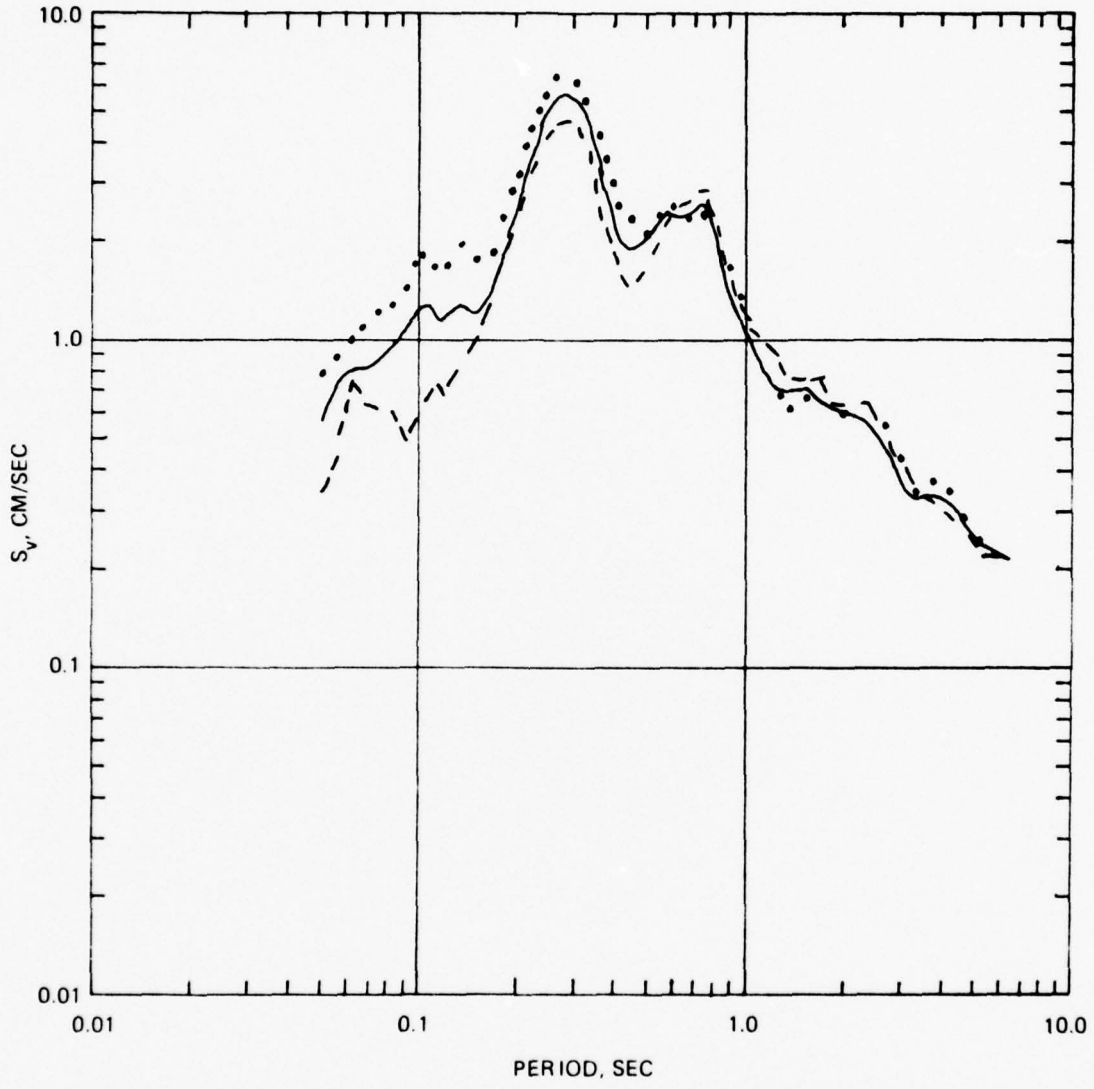

FIGURE 4.11: SPECTRA FROM BUGGY I, STATION 458 (DASHED CURVE) AND THE SUPERPOSITION WITH SCALED ALMENDRO, STATION L03, 1.375 kt (SOLID CURVE) AND 2.5 kt (DOTTED CURVE)

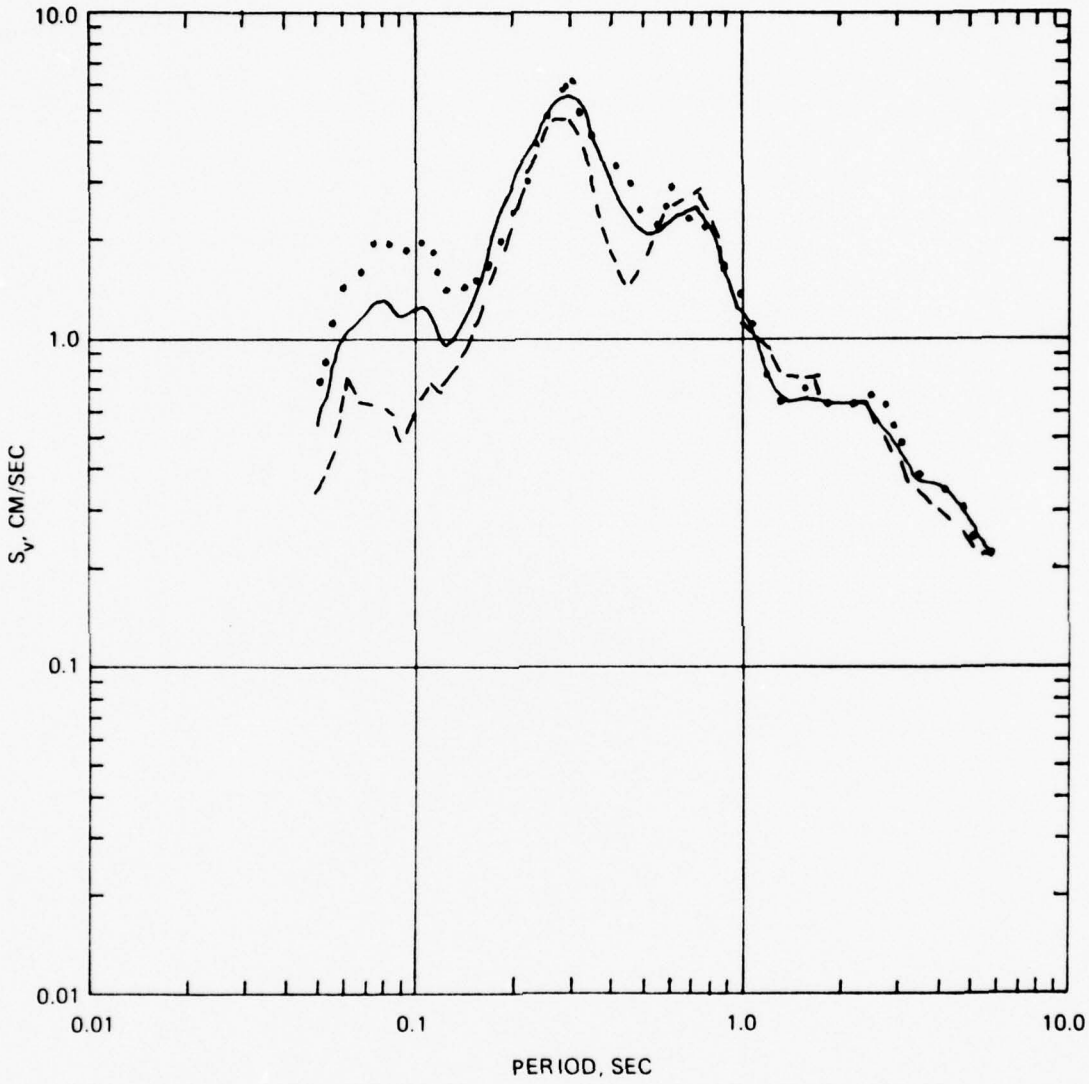

FIGURE 4.12: SPECTRA FROM BUGGY I, STATION 458 (DASHED CURVE) AND THE SUPERPOSITION WITH SCALED ALMENDRO, STATION L04, 1.375 kt (SOLID CURVE) AND 2.5 kt (DOTTED CURVE)

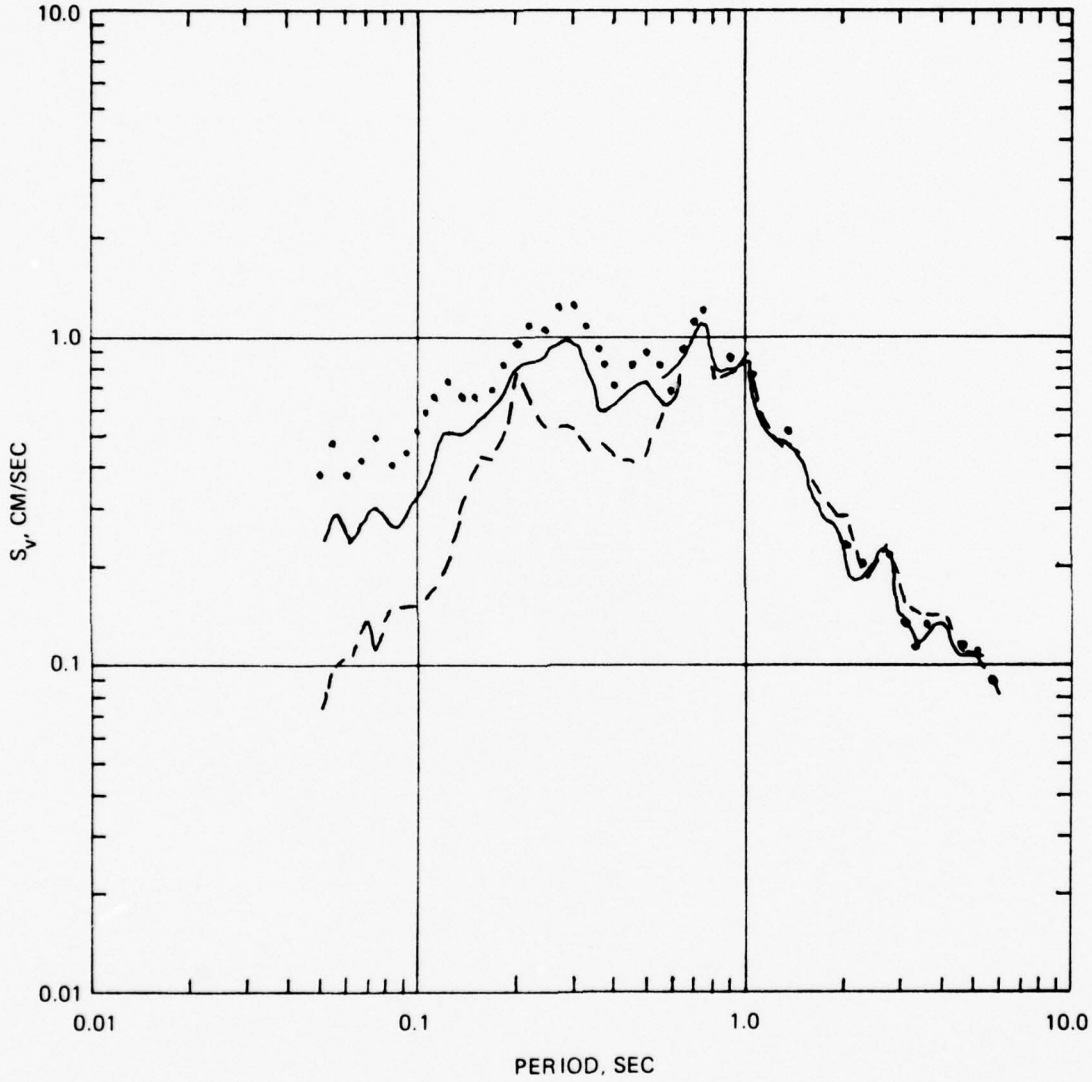

FIGURE 4.13: SPECTRA FROM BUGGY I, STATION 449 (DASHED CURVE) AND THE SUPERPOSITION WITH SCALED ALMENDRO, STATION L05, 1.375 kt (SOLID CURVE) AND 2.5 kt (DOTTED CURVE)

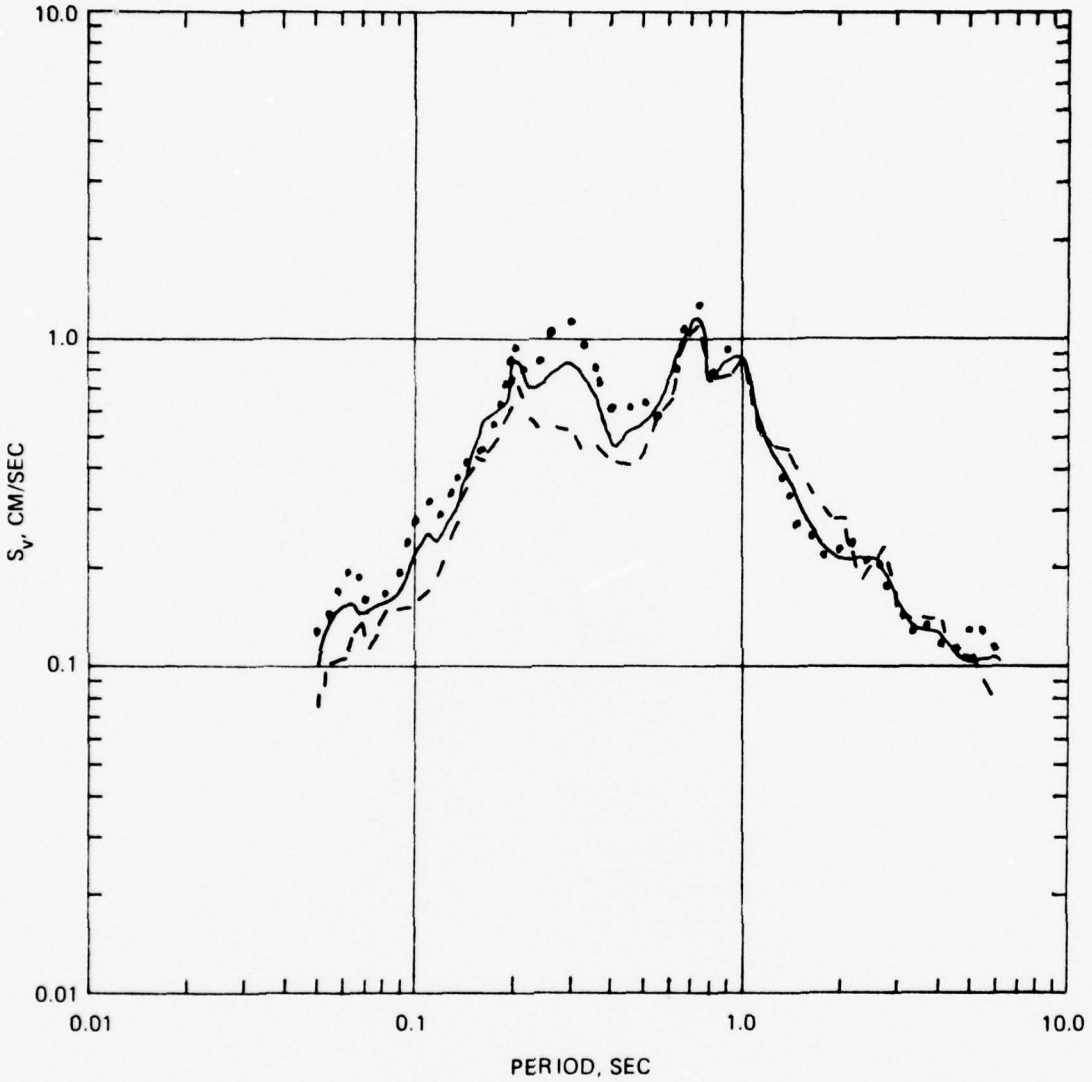

FIGURE 4.14: SPECTRA FROM BUGGY I, STATION 449 (DASHED CURVE) AND THE SUPERPOSITION WITH SCALED ALMENDRO, STATION L02, 1.375 kt (SOLID CURVE) AND 2.5 kt (DOTTED CURVE)

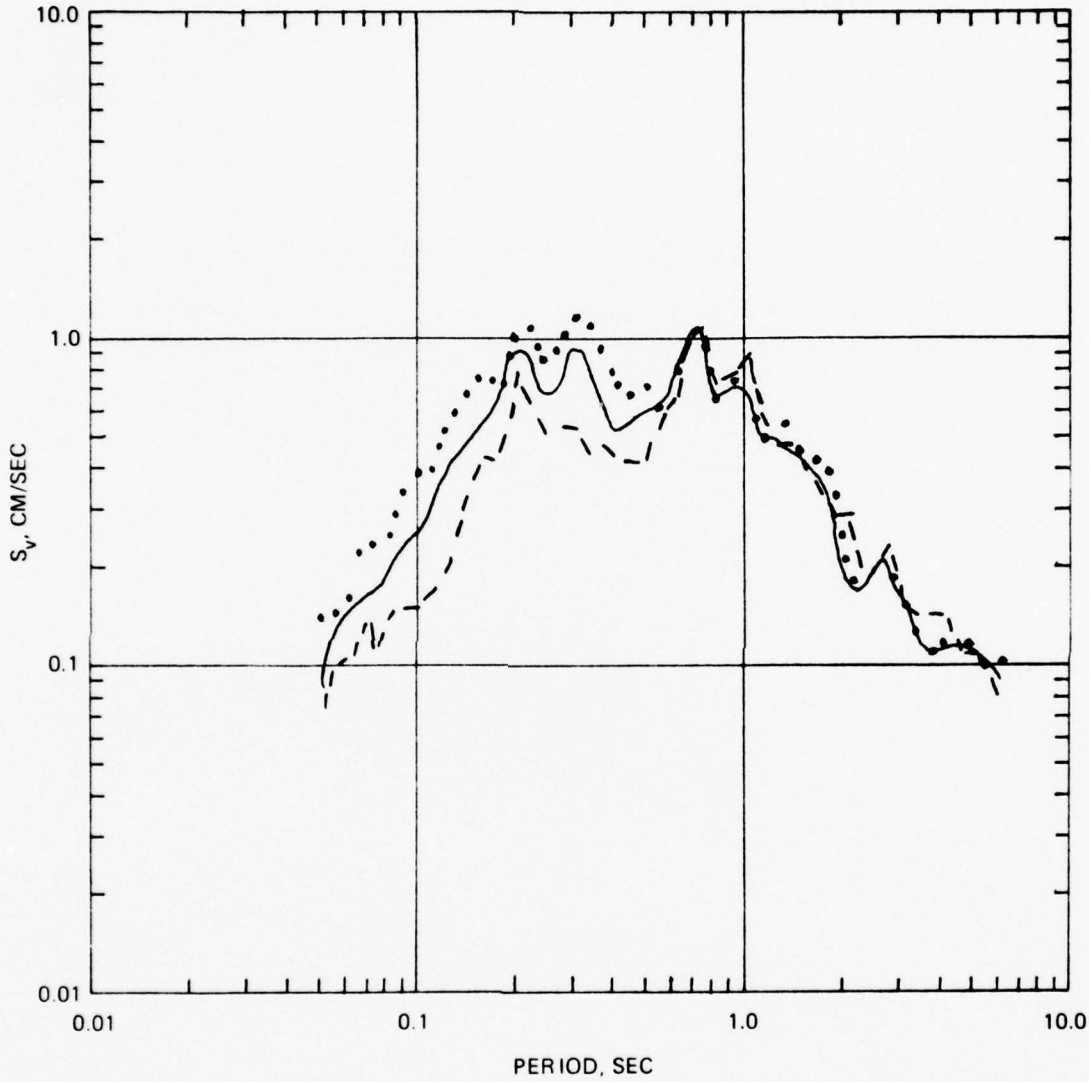

FIGURE 4.15: SPECTRA FROM BUGGY I, STATION 449 (DASHED CURVE) AND THE SUPERPOSITION WITH SCALED ALMENDRO, STATION A19T, 1.375 kt (SOLID CURVE) AND 2.5 kt (DOTTED CURVE)

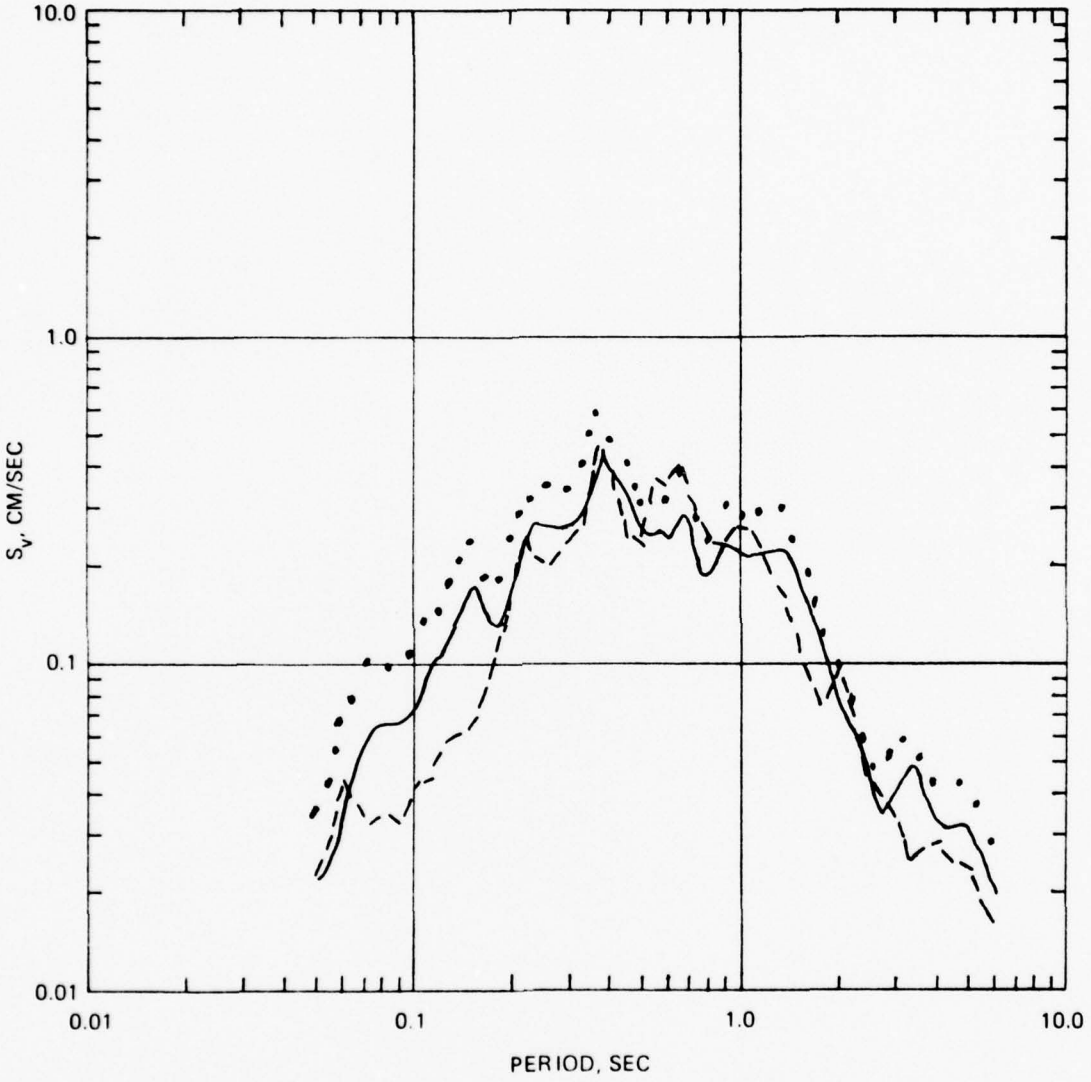

FIGURE 4.16: SPECTRA FROM BUGGY I, STATION 450 (DASHED CURVE) AND THE SUPERPOSITION WITH SCALED ALMENDRO, STATION L06, 1.375 kt (SOLID CURVE) AND 2.5 kt (DOTTED CURVE)

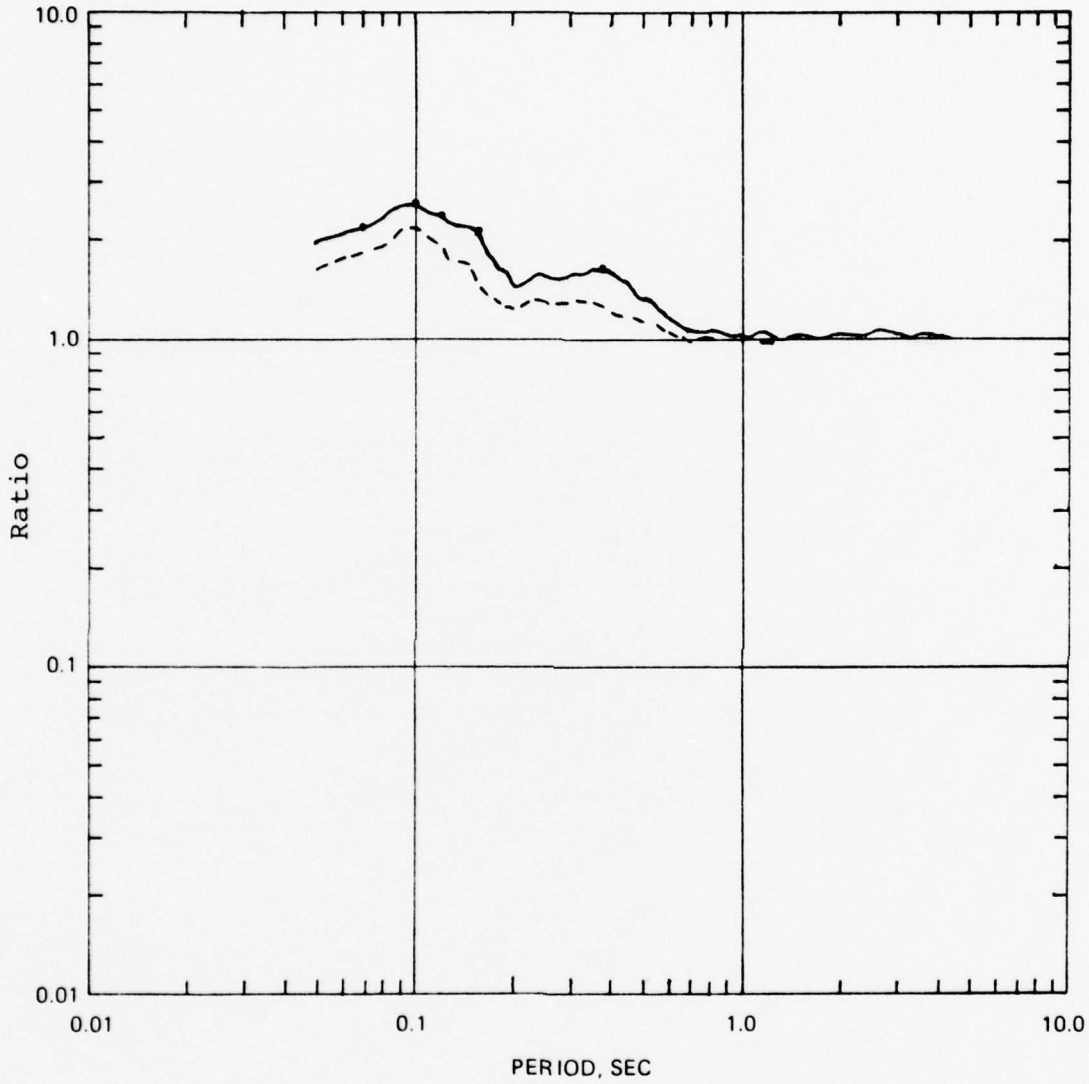

FIGURE 4.17: A PLOT OF THE AVERAGE SPECTRAL RATIO OF THE SUPERPOSITIONS USING SCALED ALMENDRO TO BUGGY I, 1.375 kt (DASHED CURVE) AND 2.5 kt (SOLID CURVE)

4.4 SUPERPOSITIONS INVOLVING SEISMOGRAMS FROM FOUR EVENTS

In addition to the Almendro Event, four NTS events (see Table 4.1) had at least one seismic recording station which approximated the source-to-station distance associated with a Buggy I station. The yields of these events ranged from less than one kt to slightly more than 50 kt, thus requiring less yield scaling than Almendro (>200 kt) to obtain the 1.375 and 2.5 kt yields necessary to simulate the evasion scenario.

The individual and superposition seismograms associated with this data sample are shown in Figures 4.18 through 4.23 for a CE yield of 2.5 kt. In general, the duration of the single contained event seismograms are comparable to or have greater duration than the Buggy I seismograms, in contrast to the relatively short duration associated with the scaled Almendro seismograms.

Spectral data from the Buggy I and superposition seismograms are shown in Figures 4.24 through 4.29 for the 1.375 and 2.5 kt yields of the clandestine event. Figures 4.24, 4.26, 4.27 and 4.29 show considerable differences between the superposition and Buggy I spectra while figures 4.25 and 4.28 show only slight differences.

Spectral ratio information for this data set is shown in Figure 4.30. It can be seen that the spectral content of the superposition is greater, on the average, over the entire period range examined. The spectral ratio is slightly greater than a factor of two at periods of 0.15 seconds (6.7 Hz) and 1.1 seconds (0.91 Hz) for a clandestine yield of 2.5 kt.

Examination of the spectral ratio from both the Almendro and the four additional events used in the superpositions indicated an increase in spectral amplitude relative to the spectral amplitude associated with Buggy I.

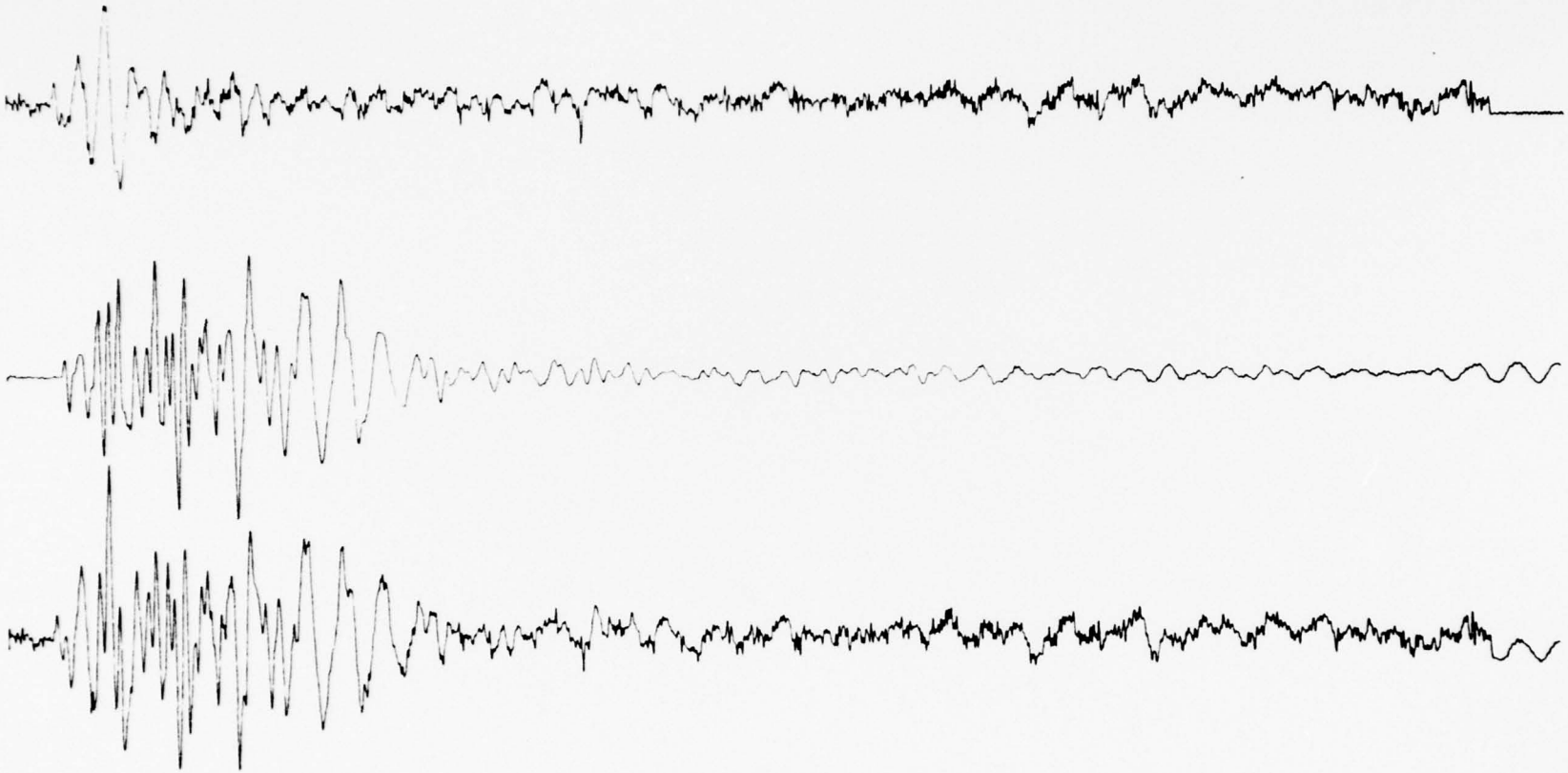

FIGURE 4.18: SEISMOGRAMS FROM BUGGY I, STATION 447 (Top Trace); SCALED EVENT A (2.5 kt), STATION 790 (Middle Trace); AND THE SUPERPOSITION (Bottom Trace)

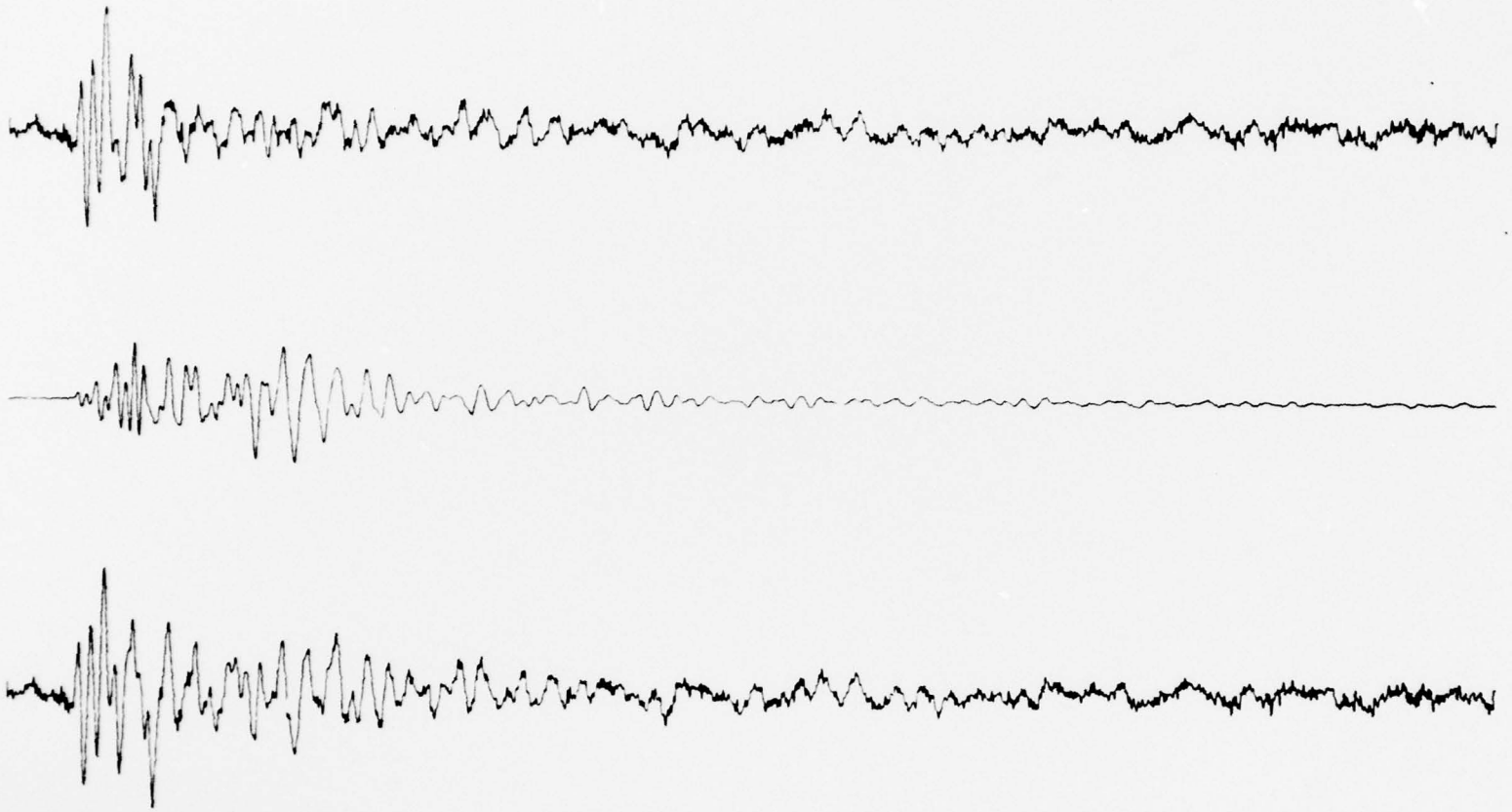

FIGURE 4.19: SEISMOGRAMS FROM BUGGY I, STATION 458 (Top Trace); SCALED EVENT A (2.5 kt), STATION 750 (Middle Trace); AND THE SUPERPOSITION (Bottom Trace)

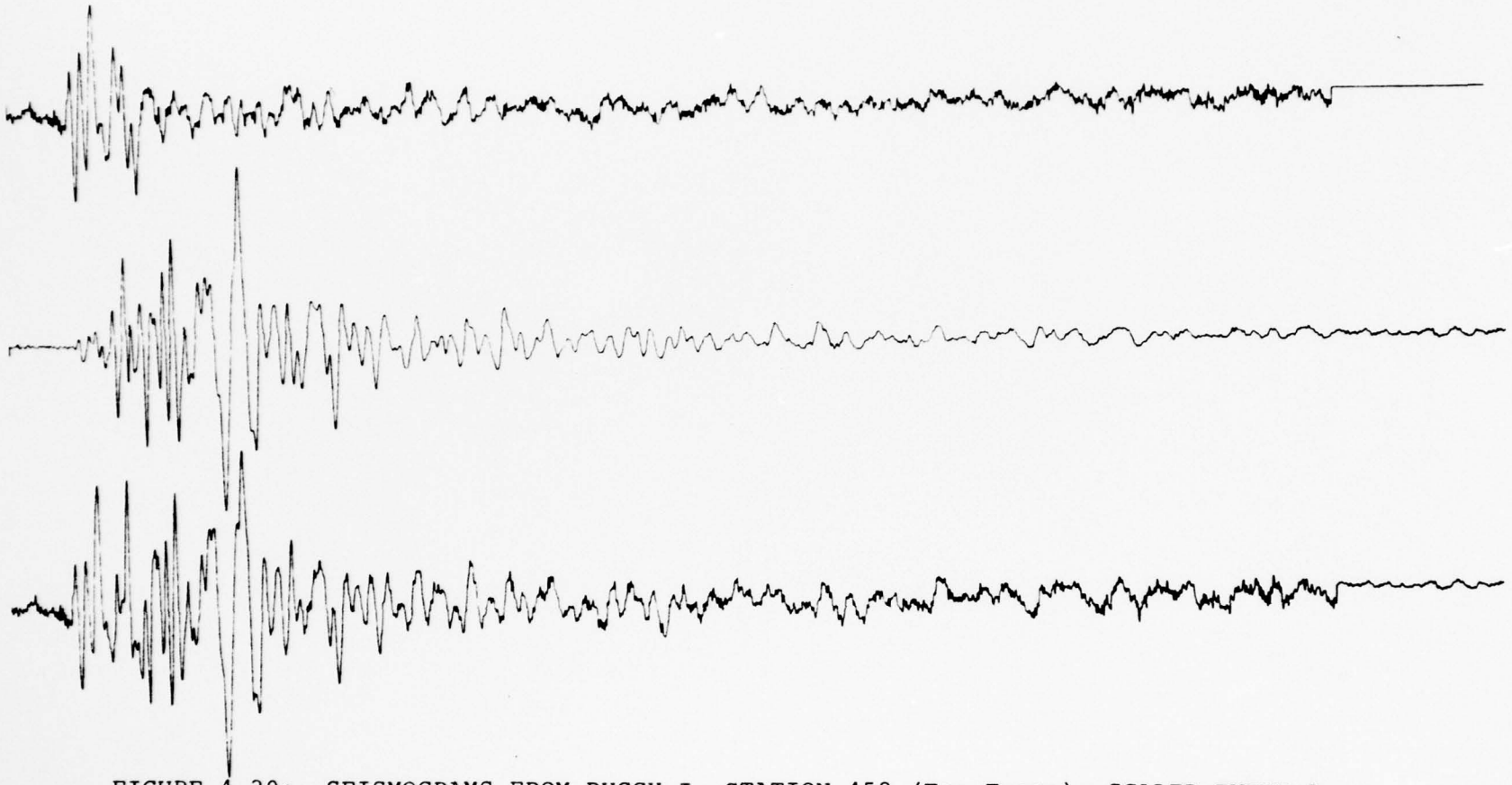

FIGURE 4.20: SEISMOGRAMS FROM BUGGY I, STATION 458 (Top Trace); SCALED EVENT A (2.5 kt), STATION 780 (Middle Trace); AND THE SUPERPOSITION (Bottom Trace)

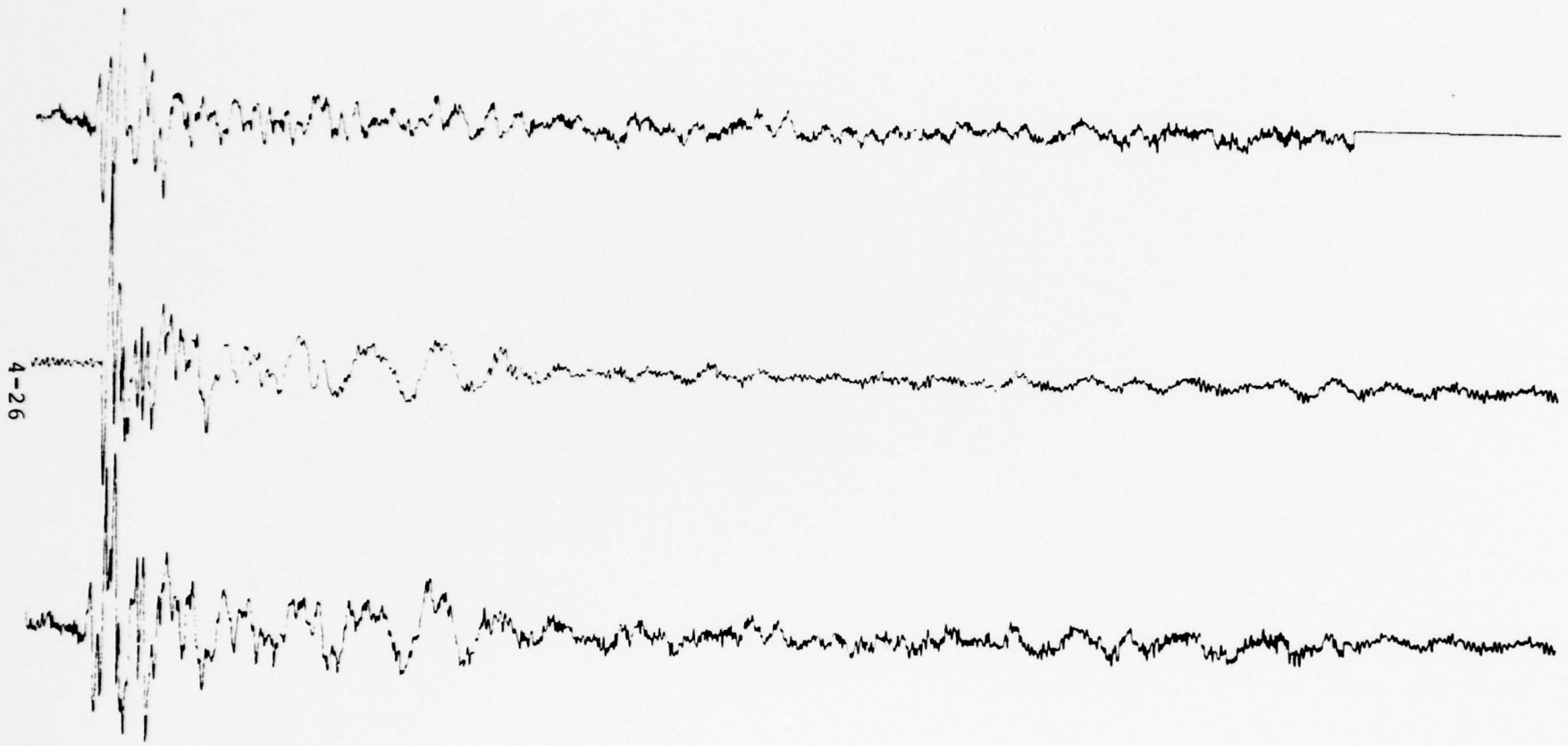

FIGURE 4.21: SEISMOGRAMS FROM BUGGY I, STATION 458 (Top Trace); SCALED EVENT B (2.5 kt), STATION L08 (Middle Trace); AND THE SUPERPOSITION (Bottom Trace)

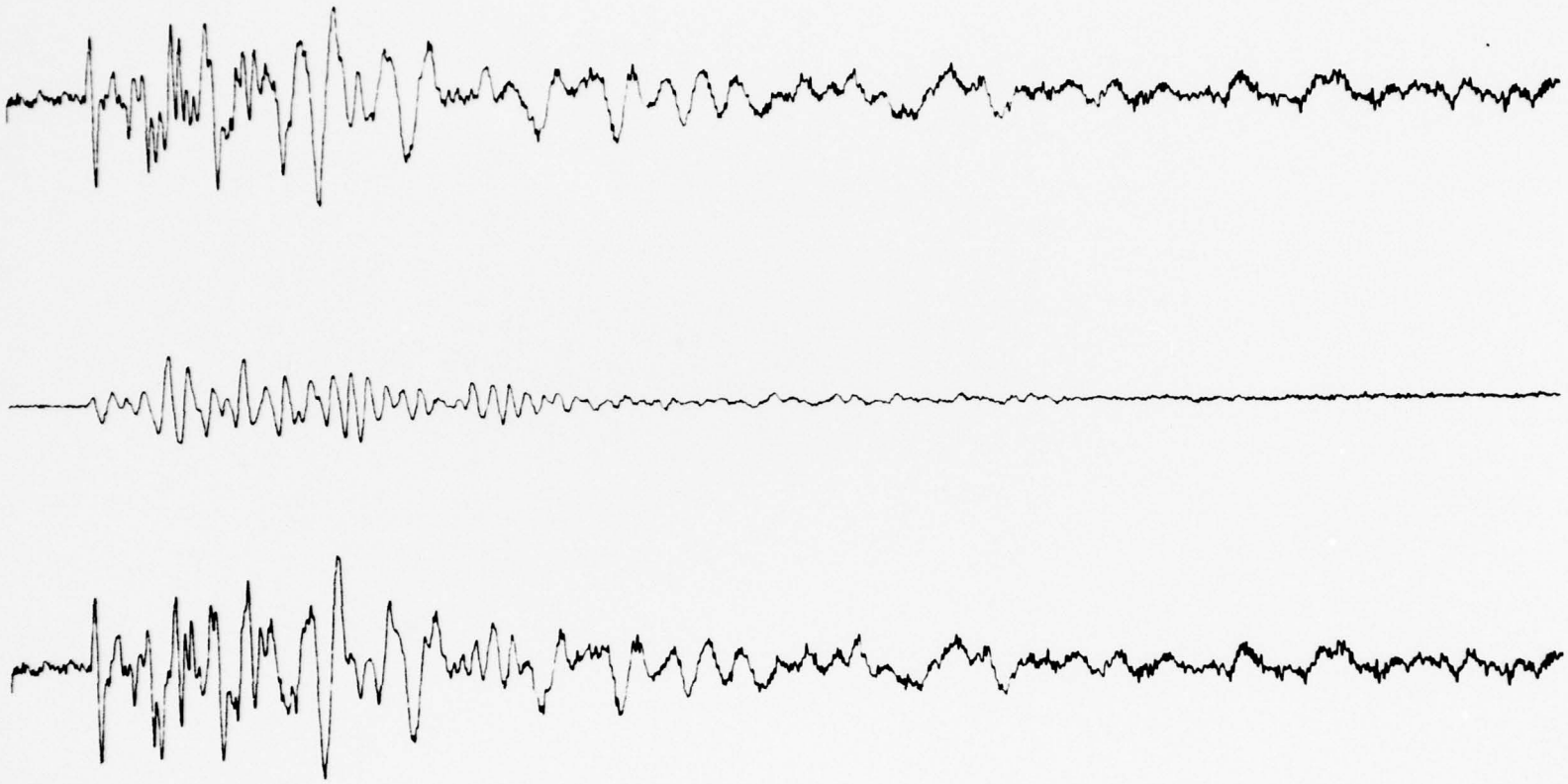

FIGURE 4.22: SEISMOGRAMS FROM BUGGY I, STATION 449 (Top Trace); SCALED EVENT C (2.5 kt), STATION 765 (Middle Trace); AND THE SUPERPOSITION (Bottom Trace)

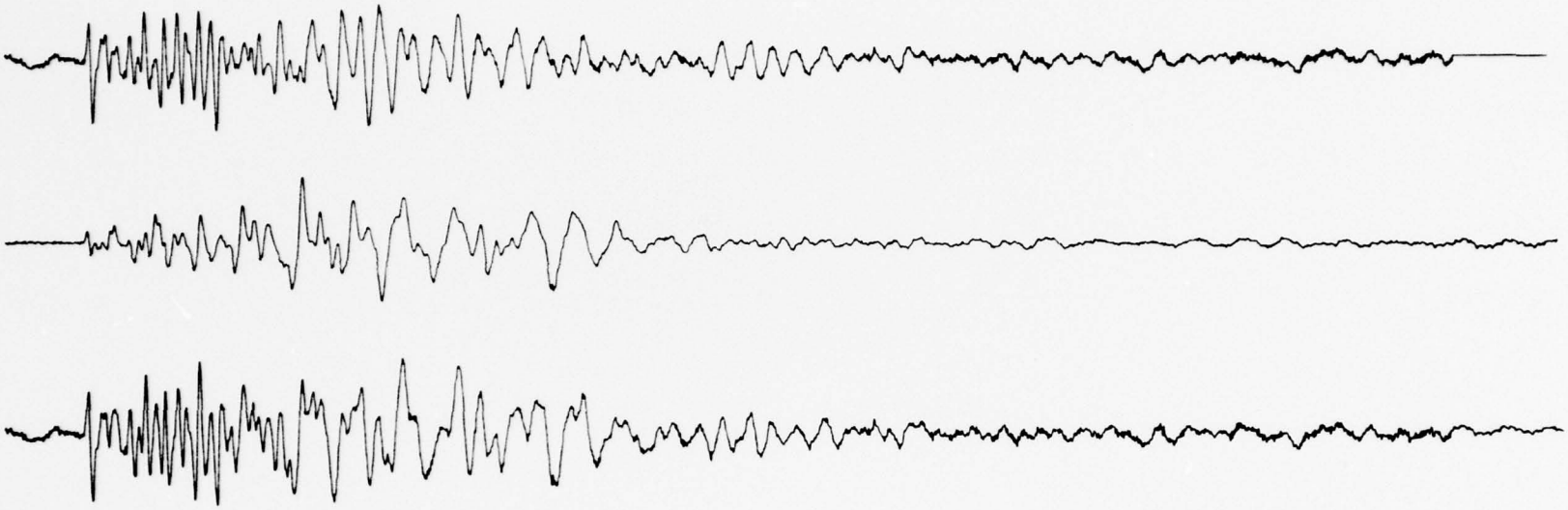

FIGURE 4.23: SEISMOGRAMS FROM BUGGY I, STATION 450 (Top Trace); SCALED EVENT D (2.5 kt), STATION CP1 (Middle Trace); AND THE SUPERPOSITION (Bottom Trace)

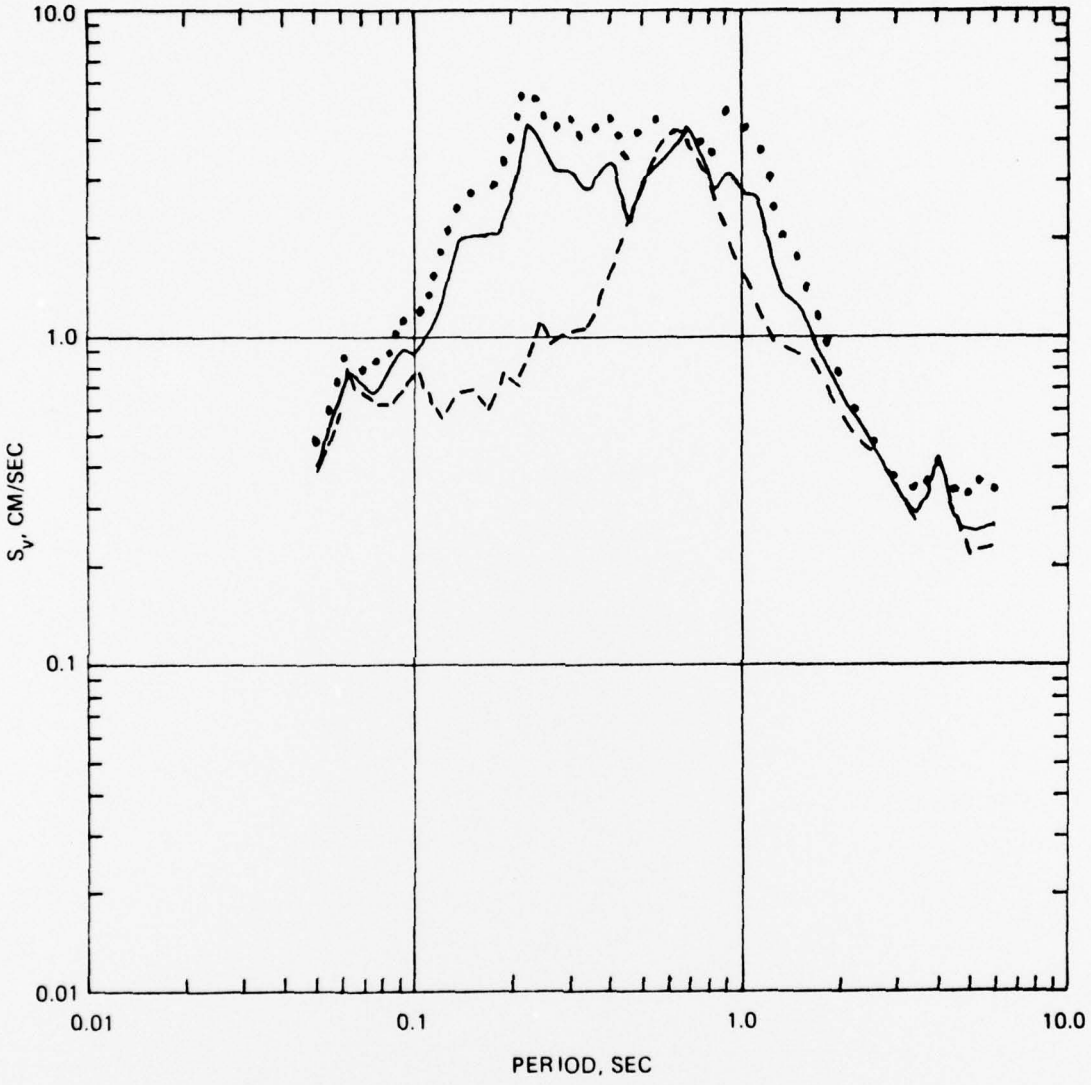

FIGURE 4.24: SPECTRA FROM BUGGY I, STATION 447 (DASHED CURVE), AND THE SUPERPOSITION WITH SCALED EVENT A, STATION 790, 1.375 kt (SOLID CURVE) AND 2.5 kt (DOTTED CURVE)

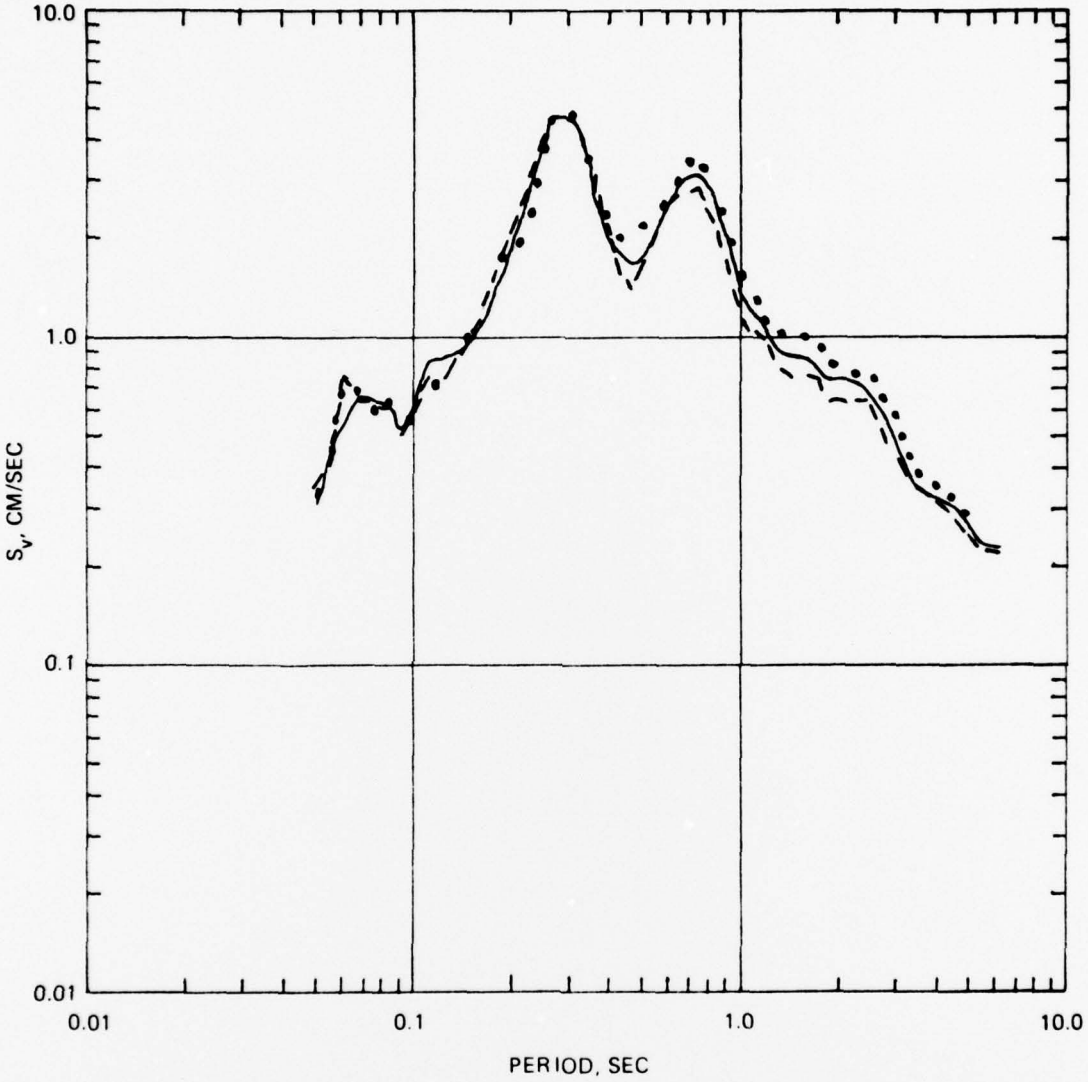

FIGURE 4.25: SPECTRA FROM BUGGY I, STATION 458 (DASHED CURVE) AND THE SUPERPOSITION WITH SCALED EVENT A, STATION 750, 1.375 kt (SOLID CURVE) AND 2.5 kt (DOTTED CURVE)

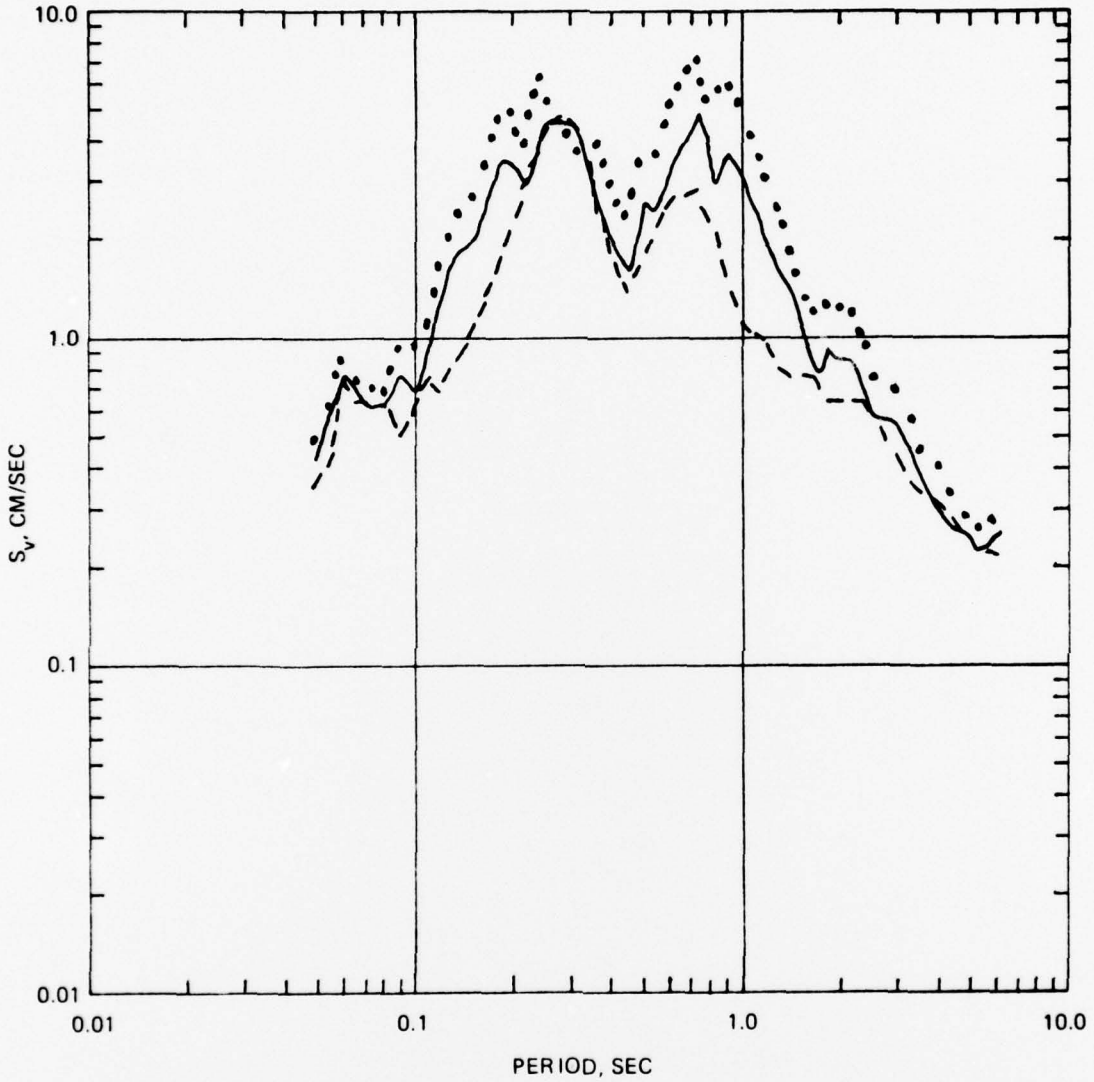

FIGURE 4.26: SPECTRA FROM BUGGY I, STATION 458 (DASHED CURVE) AND THE SUPERPOSITION WITH SCALED EVENT A, STATION 780, 1.375 kt (SOLID CURVE) AND 2.5 kt (DOTTED CURVE)

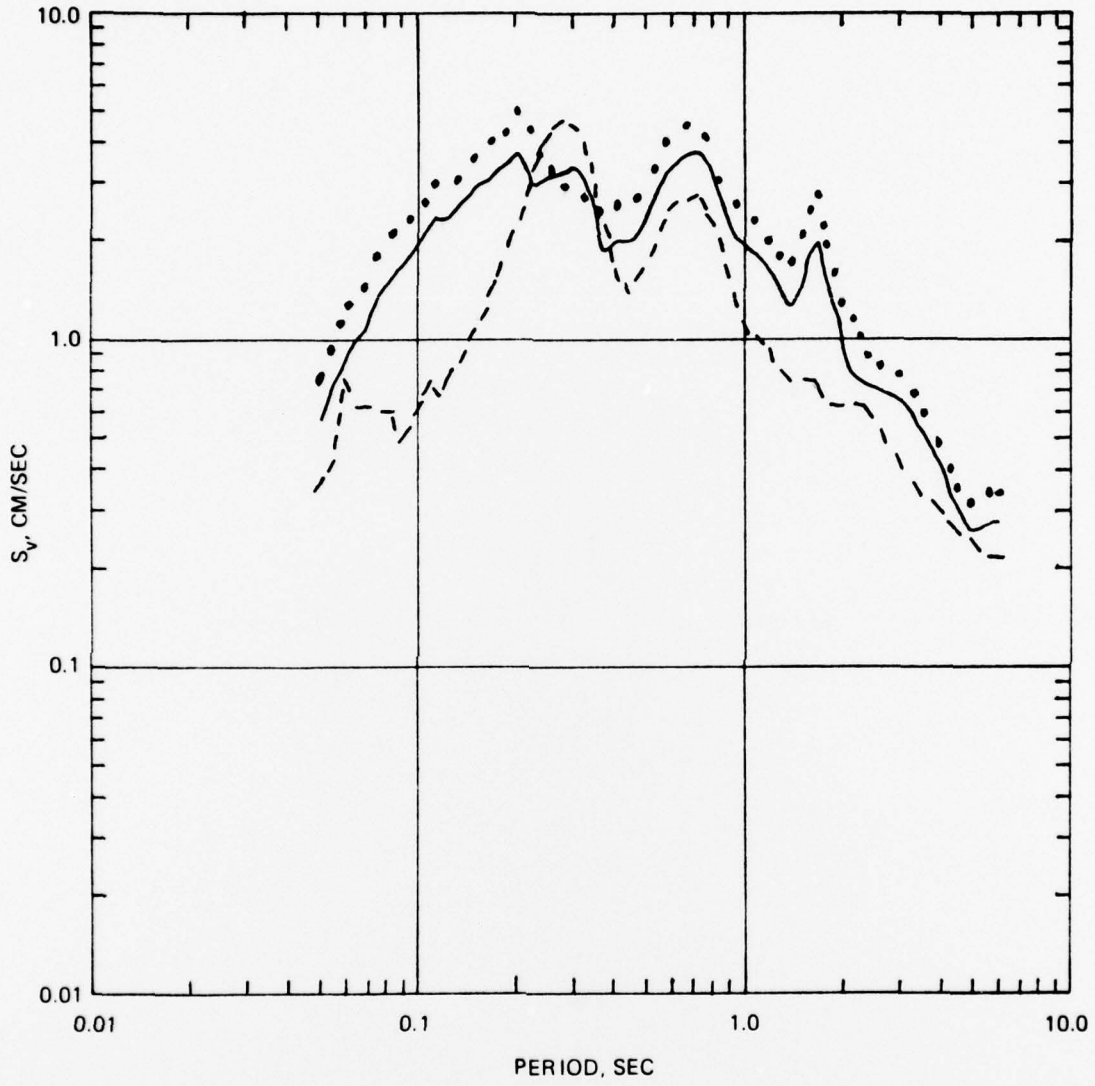

FIGURE 4.27: SPECTRA FROM BUGGY I, STATION 458 (DASHED CURVE) AND THE SUPERPOSITION WITH SCALED EVENT B, STATION L08, 1.375 kt (SOLID CURVE) AND 2.5 kt (DOTTED CURVE)

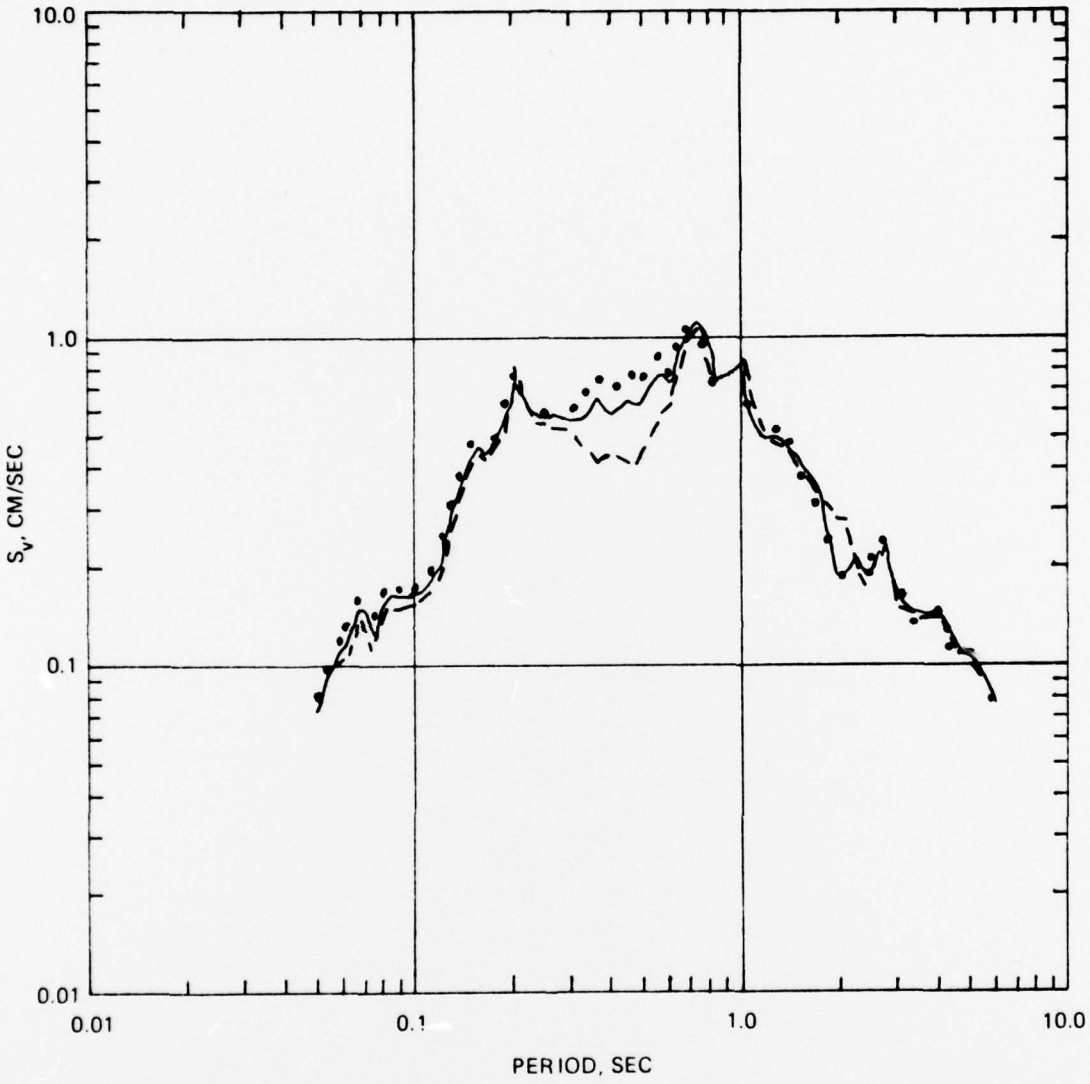

FIGURE 4.28: SPECTRA FROM BUGGY I, STATION 449 (DASHED CURVE) AND THE SUPERPOSITION WITH SCALED EVENT C, STATION 765, 1.375 kt (SOLID CURVE) AND 2.5 kt (DOTTED CURVE)

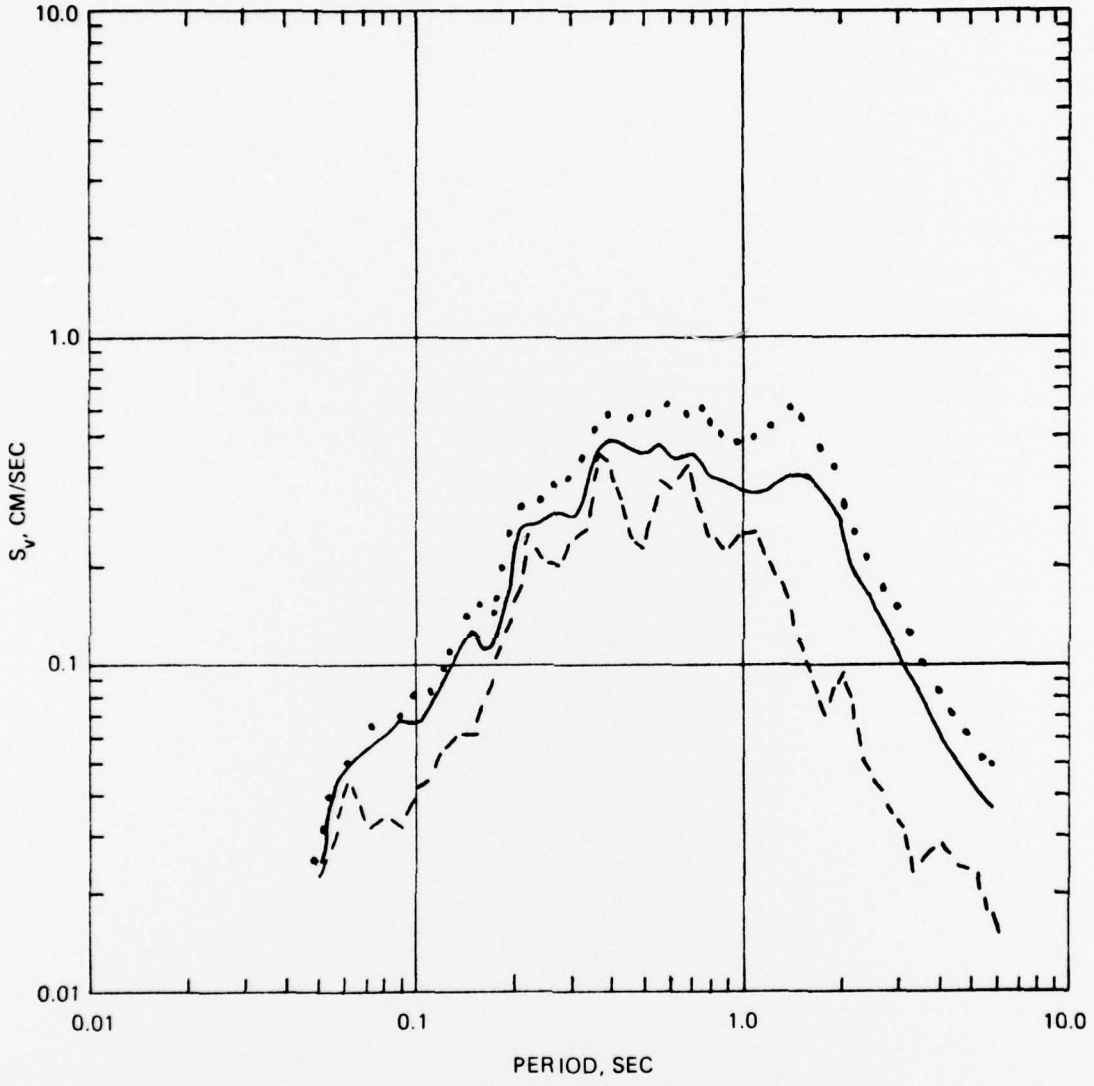

FIGURE 4.29: SPECTRA FROM BUGGY I, STATION 450 (DASHED CURVE) AND THE SUPERPOSITION WITH SCALED EVENT D, STATION CP1, 1.375 kt (SOLID CURVE) AND 2.5 kt (DOTTED CURVE)

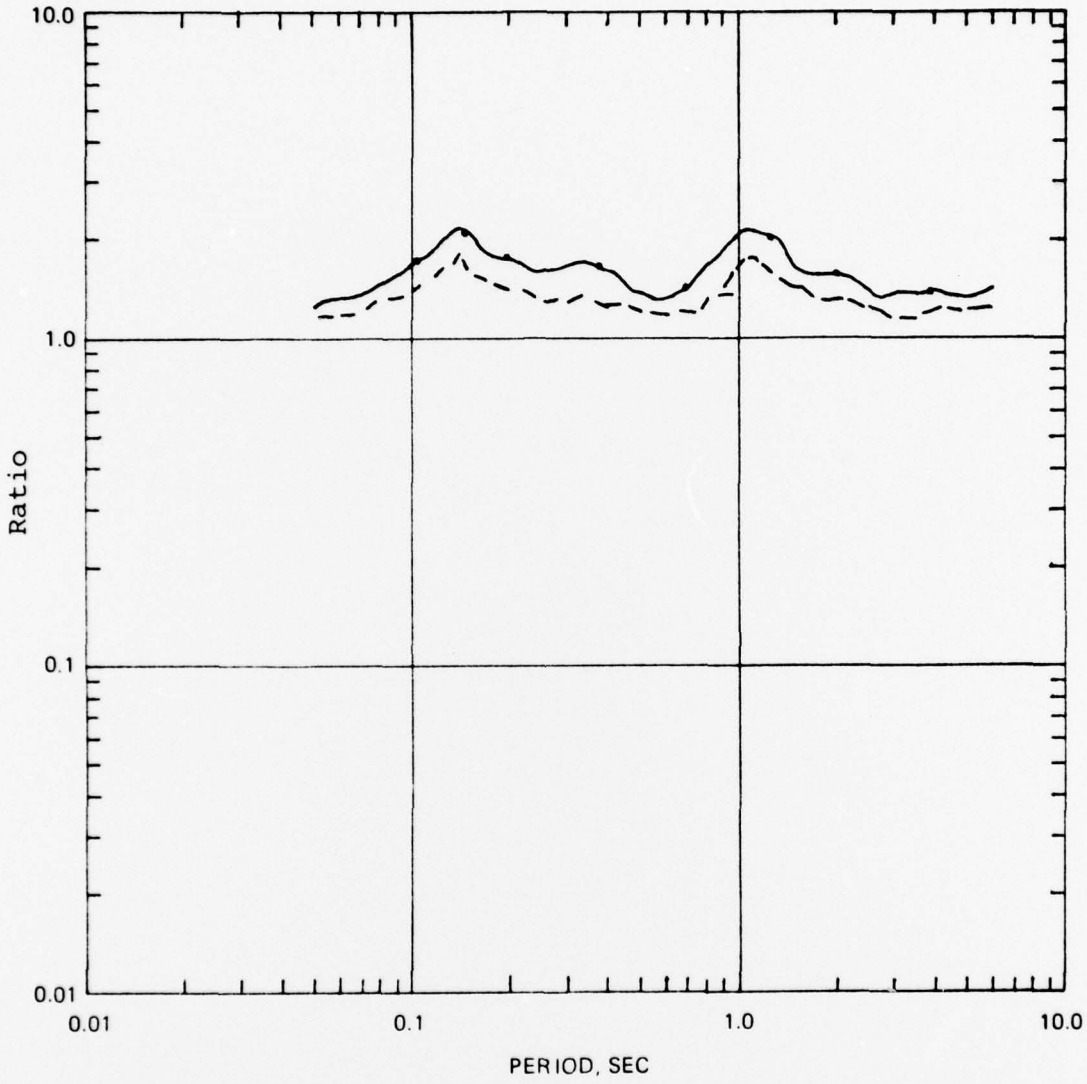

FIGURE 4.30: A PLOT OF THE AVERAGE SPECTRAL RATIO OF THE SUPERPOSITIONS USING FOUR SCALED EVENTS TO BUGGY I, 1.375 kt (DASHED CURVE) AND 2.5 kt (SOLID CURVE)

5. SUMMARY, CONCLUSIONS AND RECOMMENDATIONS

5.1 SUMMARY AND CONCLUSIONS

This report has examined the seismic aspects of a simulated PNE evasion scenario in which a single contained nuclear device is detonated in a multiple surface row-cratering environment. The constraints on the yield, detonation delay time and location of the clandestine event relative to the PNE are examined in terms of the detection capability of both far-field and on-site data. This examination indicated that the yield of the clandestine event could range from 20% to 40% of the announced PNE yield. In addition, the examination indicated that the most probable location of the clandestine event would be directed below the PNE location and that the detonation delay would range from zero to 0.3 seconds. The spectral characteristics of seismic data from a multiple surface row-cratering event are analyzed and compared to the seismic characteristics of single contained nuclear events to assess the quantitative differences between these two classes of events. Finally, the appropriate seismic data are yield-scaled and superimposed to simulate the ground motion associated with a PNE evasion, and then analyzed to determine the spectral changes caused by the clandestine event.

Based on a comparison of the spectral content of ground motion from the surface row-cratering event, Buggy I, and the spectral content of ground motion from single-contained events of equivalent yield, and on an analysis of the spectral content of Buggy I seismograms and the superposition seismograms, it is concluded that:

(1) at all periods examined, except one, the spectral amplitude content of single-contained events is, on the average, greater than the spectral amplitude of Buggy I. The maximum average spectral ratio is 2.5 at the period 0.5 sec(2.0Hz). (Figure 3.5)

(2) in the case of scaled seismic data from the Almendro event, the average spectral ratio is greater than one for periods shorter than 0.7 seconds (1.4Hz) and attains a maximum of about 2.5 (2.1) for a clandestine event yield of 2.5 kt (1.375 kt) (cf. Figure 4.17)

(3) in the case of scaled seismic data from four single-contained events, the average spectral ratio is greater than one over the entire period range examined. A short period maximum occurs at 0.15 seconds (6.7 Hz) and attains a value of 2.2 (1.8) for a clandestine event yield of 2.5 kt (1.375 kt). The spectral ratio also has a distinct peak at approximately 1.0 second (1.0 Hz) with a local maximum value approximately equal to the short period maximum. (cf. Figure 4.30).

The above conclusions are conditional, since they are based primarily on the seismic recordings from only one multiple, surface row-cratering event, Buggy I.

5.2 RECOMMENDATIONS

This study used the only available seismic data from a surface row-cratering event to represent the PNE. In order to extend this study, it will be necessary to simulate the PNE itself by using seismic data from single nuclear device events. Seismic recordings are available from surface cratering events which could be superimposed with the proper time delays to simulate an n-device surface row-cratering event. With several simulated PNE's available, a statistically meaningful set of PNE evasion scenarios could be examined and analyzed to define statistical parameters for the detection of a clandestine event in a PNE environment.

REFERENCES

1. Alewine, R.W., 1978, Personnel Communication.

2. Cassity, C.R., 1969, "Analysis of Ground Motion - Buggy I," AEC Report, NVO-1163-83.

3. Mueller, R.A. and J.R. Murphy, 1971, "Seismic Characteristics of Underground Nuclear Detonations, Part 1, Seismic Spectrum Scaling," Bulletin of the Seismological Society of America, 61, 1675.

4. Murphy, J.R., 1977, "Seismic Source Functions and Magnitude Determinations for Underground Nuclear Detonations," Bulletin of the Seimological Society of America, 67, 135.